Journal of Hydrology: Regional Studies 47 (2023) 101369

Contents lists available at ScienceDirect

Journal of Hydrology: Regional Studies

journal homepage: www.elsevier.com/locate/ejrh

Identifying driving processes of drought recovery in the southern Andes natural catchments

Jorge Vega-Briones [a,*], Steven de Jong [a], Mauricio Galleguillos [b], Niko Wanders [a]

[a] Department of Physical Geography, Faculty of Geosciences, Utrecht University, Princetonlaan 8a, Utrecht, 3584 CB, The Netherlands
[b] Facultad de Ingeniería y Ciencias, Universidad Adolfo Ibañez, Diagonal las Torres 2640, Peñalolen, Santiago, Chile

ARTICLE INFO

Keywords:
CAMELS-CL data set
Composite analysis
Random forest regression
Discharge
Vegetation
Soil moisture

ABSTRACT

Study region

The natural river basins of Chile.

Study focus

Drought effects on terrestrial ecosystems produce hydroclimatic stress with variable extensions. Particularly, hydrological drought duration can provide a better understanding of recovery together with catchment characteristics and climatology. This study focuses on the impacts of the multi-year drought experienced in Chile for more than a decade.

The recovery of relevant catchment variables to quantify the drought termination (DT) and drought termination duration (DTD) after the hydrological drought is presented. A composite analysis of natural catchments using the CAMELS-CL data set discharge (1988–2020), k-NDVI (2000–2020), and soil moisture (1991–2020) provides the average response of the recovery after severe droughts.

New hydrological insights for the region

This study demonstrates that local catchment properties can explain the recovery of studied variables after a hydrological drought.

Explanatory variables from CAMELS-CL to derive the DT using random forest regression (RFR) were used with a strong correlation of 0.92, 0.84, and 0.89 for discharge, vegetation productivity, and soil moisture, respectively.

The discharge patterns show longer recovery over environments dominated by shrublands with less precipitation and higher temperatures, in central Chile, while higher latitudes with higher vegetation cover, increasing precipitation, and lower temperatures present shorter recovery times. The vegetation productivity shows longer recovery over highly vegetated mountains in central Chile. The soil moisture recovery spatial distribution presented patterns that connect them with the discharge recovery. This work enables the identification of drought vulnerability, which is valuable for managing water resources and ecosystems and is helping to predict drought recovery periods in regions with a lack of observations.

1. Introduction

Drought causes hydroclimatic stress on terrestrial ecosystems and its impacts are expected to increase due to changes in precipitation patterns and rising temperatures related to climate change (Wanders and Wada, 2015; Van Loon et al., 2016; Prudhomme et al., 2014; Samaniego et al., 2018; Ovenden et al., 2021). Terrestrial ecosystems play a vital role in the global carbon, water, and

* Corresponding author.
E-mail address: j.e.vegabriones@uu.nl (J. Vega-Briones).

https://doi.org/10.1016/j.ejrh.2023.101369
Received 20 July 2022; Received in revised form 20 March 2023; Accepted 21 March 2023
Available online 3 April 2023

energy cycle, however, the increasing intensity and frequency of droughts are affecting their behavior and recovery (Cartwright et al., 2020; Piao et al., 2013; Xi and Yuan, 2022). Drought is usually defined as below-normal water availability, and generally classified according to the meteorological, hydrological, agricultural, and socioeconomic perspective (Tallaksen et al., 2004; Wilhite and Glantz, 2019; Van Loon, 2015). Specifically, hydrological drought is associated with a lack of water in the hydrological system such as rivers, lakes, and groundwater. The propagation of meteorological drought over the terrestrial hydrological cycle determines the hydrological drought, influenced by the cycle properties (Peters et al., 2006; Van Lanen, 2006; Vidal et al., 2010). The impacts of a drought are usually subjected to the severity and duration of the hydrological drought event, which can be expressed by streamflow drought duration or deficit volume (Van Loon, 2015). Meanwhile, the life cycle of hydrological drought considers the development from the onset to the maximum intensity, and the recovery is referred to as the maximum intensity to complete recovery (Wu et al., 2020).

During the last decades, multiple drought events with high severity and duration resulted in extreme impacts on water resources, such as low river discharge, groundwater, and reservoir levels. This may lead to different implications for terrestrial ecosystems and human water consumption such as severe wildfires, human migration, hunger, loss of life, restriction of water use for irrigation, and lack of domestic water (Van Loon, 2015). Several examples of multi-year drought evidenced these impacts, such as the 2010 drought in Brazil which presented a high impact on their terrestrial ecosystems. Human consumption problems in Australia between 2002 and 2010, California (USA) between 2013 and 2014 (Sheng and Xu, 2019; Williams et al., 2015), and in Europe between 2003 and 2006 (Van Loon, 2015). Chile is experiencing a multi-drought period with a large temporal and spatial extent. Its causes have been mostly attributed to anthropogenic climate change, contrasting with "La Niña" conditions that often accompanied past droughts (Garreaud et al., 2020; Boisier et al., 2016). This period of water stress may lead to faster impacts on hydroclimate and terrestrial ecosystems by altering their composition, structure, and function (Zhang et al., 2021; Vicente-Serrano et al., 2013, 2015; Wu et al., 2018).

Furthermore, the extreme precipitation deficits (up to 45%) affected important natural resources, including natural vegetation, crops, and water supply (Alvarez-Garreton et al., 2020; Garreaud et al., 2017). Garreaud et al. (2017) showed that this precipitation deficit diminished the Andean snow pack and resulted in amplified declines (up to 90%) of river flow, reservoir volumes, and groundwater levels along central Chile. Decreases in water supply would be exacerbated within the multi-year drought period as well. Alvarez-Garreton et al. (2019) modeled the impacts on water supply due to afforestation with different combinations of native forest and forest plantations predicting a decrease in mean annual runoff in central-south Chile catchments. Also, less water supply is shown in catchments with snow accumulation due to multi-year drought-increasing propagation (Alvarez-Garreton et al., 2020).

In natural areas, the alteration of ecosystem metabolism due to water shortage can change the carbon sink dynamics triggering positive climate feedback, leading to a reduction of carbon uptake, or to a restoring function that recovers after the drought is ameliorated (Beer et al., 2010; Heimann and Reichstein, 2008; Qie et al., 2017). The impacts on forests due to droughts enhanced by climate change are producing negative effects on Mediterranean sclerophyllous forests (Miranda et al., 2020) and also affecting their future development with a decline projection of growth for the coming decades in forests dominated by endangered species (Matskovsky et al., 2021).

Climate change is likely to affect atmospheric feedback and increase drought impacts on terrestrial ecosystems (AghaKouchak et al., 2021; Pugnaire et al., 2019). The increase in the demand for evaporation and reductions in water availability will reduce the vegetation's resilience against future drought events (Vicente-Serrano et al., 2013; Gazol et al., 2018). In the case of Chile, as a result of reductions in precipitation up to 30% under the most extreme scenario of IPCC (RCP8.5), it is projected up to 40% reductions in runoff as well (Bozkurt et al., 2017; Valdés-Pineda et al., 2016). In addition, central Chile had an important land cover change over the last 50 years, showing a consistent decrease in the annual runoff with increments of forest plantations, at the expense of natural vegetation which can influence the recovery of the catchment with high land cover change during this period (Lara et al., 2012).

Drought monitoring and the analysis of the discharge, vegetation, and soil moisture recovery are important for policymakers and public use because the increasing impacts of climate change are connected with the hydrological cycle (Masson-Delmotte et al., 2021). Therefore, innovative studies applying methods such as composite analysis (CA), can provide new insights and robust descriptions of drought events and drought recovery patterns (Xie et al., 2017). The full drought recovery is defined by Gessler et al. (2020) as the capacity of ecosystems to return to the undisturbed ecosystem state and functioning following a drought disturbance. In this regard, studying the length and periodicity of droughts is crucial to understanding the post-drought recovery time (RT) and for evaluating drought effects (Zhang et al., 2021; Schwalm et al., 2017; Xi and Yuan, 2022).

The post-drought recovery times across various ecosystems are still controversial and not clear to the scientific community, where a consensus on the understanding across global ecosystems and factors influencing post-drought RT has not been reached yet. A recent study from Xi and Yuan (2022) shows that ecosystem response, represented by Gross Primary Productivity on the onset and recovery stage, has significant water stress from soil moisture and vapor pressure deficit during flash droughts. This study also provides information to understand the implications of these impacts on the hydrological cycle.

In addition, in previous studies, the definition of drought events, mostly stands on the meteorological drought index which, is not necessarily associated with stress to the ecosystem (Vicente-Serrano et al., 2013). This study intends to answer this, relating the stress on the ecosystem by identifying hydrological drought, and applying a composite analysis that includes key ecosystem variables as a novel approach.

In this study, we aim to (1) quantify the length of the drought recovery in their extension and magnitude, (2) identify spatial patterns related to drought recovery, and (3) analyze and relate drought events to environmental factors such as hydrological properties.

2. Methods

In this study, we looked at the impact of climate and catchment properties on drought recovery in natural undisturbed catchments in Chile. To this end we used the extensive catchment data set for large sample studies, specifically created for Chile between the latitudes −17.8 and −55.0° S (CAMELS-CL, Alvarez-Garreton et al., 2018). The discharge from CAMELS-CL (1988–2020) for the hydrological drought identification was supplemented by vegetation productivity represented by the k-NDVI index from MODIS (2000–2020), and soil moisture from ESA CCI-SM (1991–2020) to determine Drought Termination (DT) and Drought Termination Duration (DTD). The MODIS satellite retrievals at a daily time scale, strengthened by the recently developed kernel-NDVI (kNDVI) were used to obtain the vegetation productivity (Justice et al., 2002). This index is able to improve the representation of plant behavior compared with other vegetation indices. The ESA CCI soil moisture products (Preimesberger et al., 2021) provides also a robust data set for recovery analysis, which uses active/passive satellite retrievals at a daily scale with global coverage. The spatial distribution of DT/DTD was analyzed using a range of explanatory variables in combination with Multiple Linear Regression (MLR) and Random Forest Regression (RFR) to explain the observed spatial patterns. In this section, a description of the study area and the identification method of drought events is provided. The acquisition of remote sensing data, followed by the conceptual framework of the composite analysis and drought termination is defined. Finally, the determination of explanatory variables is explained.

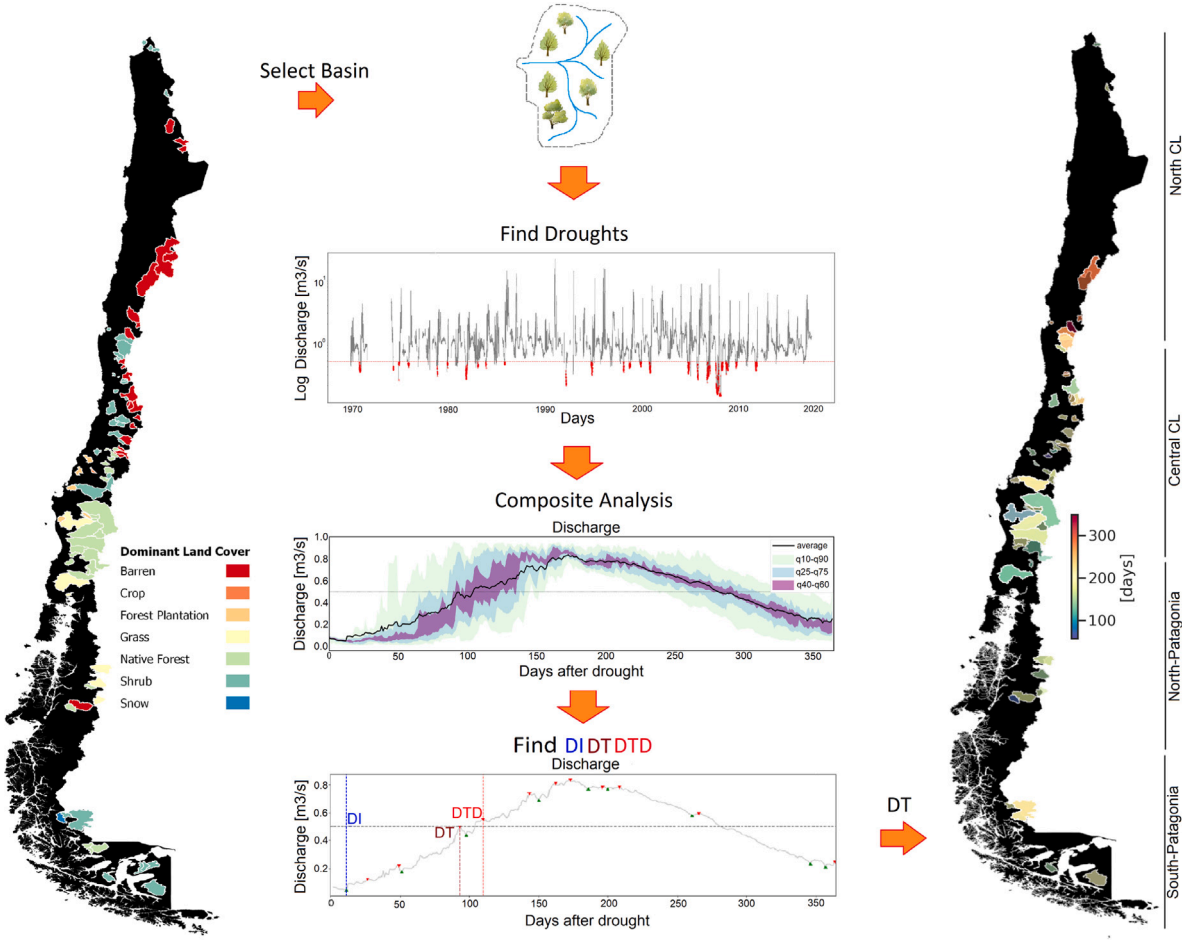

Fig. 1. Study area and flow diagram of DI, DT, and DTD analysis. The left side shows the catchment distribution characterized by their dominant land cover. The center, shows the drought identification, composite analysis, and termination recognition. Right side, show the discharge DT distribution.

2.1. Study site

The study site is located in the southwest of South America, with a distinct geographical configuration, and covers a latitudinal range of 4300 km from North to South (Fig. 1). A total of 163 natural catchments (out of 516 from CAMELS-CL) were used for this study (as dots in Fig. 1). The catchments selected as "natural" presented over 80% of the discharge observations between 1988 to 2020 without the presence of dams that alter discharge behavior (Alvarez-Garreton et al., 2018). Two mountain ranges are featured from West to East separated by the intermediate depression, namely the coastal range (500–2.200 m.a.s.l.) and the Andes mountains (4000–7.000 m.a.s.l.) (Fernández and Gironás, 2021). The precipitation regimes are strongly influenced by the Andes barrier effect

for atmospheric flows at high elevations, particularly in the south of Chile. The elevation of the gauge stations ranged from 5 to 4.539 m.a.s.l. The study area is located, along a climate gradient of particular importance and interest for conservation and food security, due to its high levels of biodiversity, life forms, and agriculture diversity (Mittermeier et al., 2004).

The vegetation composition varies in latitude and longitude through this climate gradient. At the lowest latitudes, the presence of arid and semi-arid shrub lands dominate changing to Mediterranean Forest to the South, transitioning to a Temperate Forest and peat bogs towards the high latitudes (Luebert and Pliscoff, 2017). This variation is also influenced by longitude due to the Andes and Coastal mountain range, where sun exposition and coast humidity play an important role in water availability and vegetation composition (Urrutia-Jalabert et al., 2021; Miranda et al., 2020). The valleys are dominated by agricultural fields, while over the mountains native forest and forest plantations are located (CONAF, 2018).

The climate and weather of this region are strongly influenced by the semi-permanent subtropical anticyclone over the Southeast Pacific (SEP) and the westerly wind regime at mid-latitudes creating a north–south precipitation gradient. The climate ranges from hyper-arid and semi-arid in the north, to the Mediterranean with a marked dry period in spring–summer in the center. A temperate climate with Mediterranean influences is present in the South. The climate has been drying and warming up over the last decades across south-central Chile (Fernández and Gironás, 2021; Urrutia-Jalabert et al., 2021; Luebert and Pliscoff, 2017).

The precipitation volumes show a significant negative trend since 2010 with a reduction of 25%–45% in annual precipitation (Garreaud et al., 2020). This tendency is attributed to the Pacific "Blob" described by Garreaud et al. (2021) providing a decade-long rainfall deficit in Central Chile, accompanied by an above-normal frequency of heat waves and more intense fire seasons (González et al., 2018).

2.2. Remote-sensing data

2.2.1. Vegetation data

The kernel-NDVI (kNDVI) index was obtained from the combined MODIS Collection (MCD43A4 Version 6 Nadir Bidirectional Reflectance Distribution Function-Adjusted Reflectance) to assess vegetation productivity at a daily temporal resolution (NASA, 2022). The kNDVI (Camps-Valls et al., 2021) is closely related to the Gross Primary Productivity (GPP) which is an important indicator of carbon fixation during photosynthesis. This kernel-NDVI method aims at overcoming the linear approach of the conventional NDVI (Normalized Difference Vegetation Index) by accounting for the non-linear behavior of spectral indices with biomass or leaf area index. The kNDVI derives an automatic and pixel-wise adaptive stretching, keeping the relation between near-infrared and red channel, allowing it to cope with saturation effects, complex phenological cycles, and seasonal variations, to deal with the mixed-pixel problem, and to propagate lower uncertainty than other indices (Camps-Valls et al., 2021). The equation of the kNDVI is given by:

$$kNDVI = tanh((NIR - red/2\sigma)^2) \tag{1}$$

where σ is a length-scale parameter to be specified in each particular application and represents the sensitivity of the index to sparsely/densely vegetated regions. The MODIS products have 500 m resolution and are available since 2000 (Didan et al., 2015).

2.2.2. Soil moisture data

The combined CCI-Soil Moisture product (v04.7) based on Level 2 products for both passive and active retrievals was used to assess the first 10 cm of the water content of soil (Preimesberger et al., 2021; ESA, 2021). The resolution of this product corresponds to 0.25 degrees, at a daily time step. The data was processed with a python algorithm to obtain the spatial average values for each catchment in the study area.

2.3. Composite analysis

Composite Analysis (CA) was developed by Chree (1913, 1914) originally for space science, however, is widely used in different fields of earth science (e.g. Xie et al., 2017; Nicolai-Shaw et al., 2017). Also, referred to as superposed epoch analysis and conditional sampling, the CA is used to comprehend the relationship between different phenomena and hydrological variables. CA involves collecting large numbers of cases of a given meteorological phenomenon, in this case, drought events. These cases are composited together as a collection (for each variable and catchment), perhaps with different types of stratification, using one or more covariates that are suspected to have an influence on the phenomenon. The composite analysis then generally involves computing the composite mean and some other statistical measures, such as the standard deviation and statistical significance. The resulting structures which emerge can tell a powerful story about how that phenomenon is affected by the factors used in the composite stratification. In the case of drought events, a negative response to droughts from discharge, vegetation productivity, and soil moisture is expected for a year after the event. If drought events satisfy our selection criteria (in the section Definition of drought events), the timing of those events is selected as key times and grouped per catchment. Later, the drought response signal for each of the variables is isolated by calculating the average drought behavior in time, over which the DT and DTD are determined. Due to the spatial resolution of vegetation (500 m) and soil moisture (27–28 m), the average composite analysis per catchment presents higher variability for soil moisture.

Finally, with the implementation of statistical tests, we defined if there is a significant (lagged) connection between the variables. This process enhances the signals as a result of the extraction of events while noises are averaged out (Xie et al., 2017).

The normalization was performed with the empirical cumulative distribution function of the data (Dekking et al., 2005). The signal of variables with lower values is assessed better by accumulating the values close to zero due to the very steep curve of the function near zero that flattens out towards higher values. This is especially relevant for low discharge, vegetation, and soil moisture measurements during drought periods. The function provides the proportion of elements in the data set that are less than or equal to x:

$$F_n = \frac{\text{number of elements in the data set} \leq x}{n} \tag{2}$$

2.4. Definition of drought events

A fixed threshold approach was used to define hydrological drought events with a fixed percentile threshold of 80% for the daily streamflow anomalies between 1988 to 2020, following Wanders and Wada (2015), and Van Loon et al. (2016). These drought events were established for each catchment as key times in this study.

2.5. Determination of drought termination and drought termination duration

Drought termination can be characterized by its duration, rate of recovery, and seasonality (Nkemdirim and Weber, 1999; Mo, 2011; Parry et al., 2016). In this regard, the ensemble mean from the CA was used to identify the Drought development and Drought Termination. Fig. 1 shows the location of the study area with the size of the catchments (left), a flow diagram of the CA-analysis (center), and the drought termination in days (right). The first day of the drought termination corresponds to the day when a minimum peak is reached after the drought event starts (DI in Fig. 1). The drought ends when the signal exceeds the Q80 threshold, however, the last day of the drought termination (DT) phase is found when the normalized threshold of 0.5 is reached. This threshold is selected due to the normalization method (Dekking et al., 2005) which performs normalization on sorted data, and later brings data back in place based on the original index, as defined by Parry et al. (2016). The drought termination duration (DTD) corresponds to the first recovery peak after crossing the normalized discharge threshold of 0.5, with a window of seven days. These days after drought termination are added to the recovery because the basin needs more time to replenish flow deficit (Mo, 2011; Parry et al., 2016). Furthermore, the window of seven days gives enough time to show a recovery peak and is based on half of the period used by Ahmadi et al. (2019a) to classify discharge drought recovery (US). A group of drought events can provide an average termination phase in days between DI and DT, while the DTD is the number of days between DI and DTD. (Parry et al., 2016).

The differences between DT and DTD recovery rely on the identification method considering the recovery threshold at 0.5. The DT corresponds to the period between the minimum peak of the hydrological drought until it reaches the threshold. In comparison, DTD is the period between the lower peak after the drought starts and the first peak after the threshold. The lower and upper peak is defined as a window of seven days where there is an increase and a reduction (upper peak) of the signal. The presence or absence of snow between catchments was determined by the "soil water equivalent" from the CAMELS data set.

2.6. Explanatory variables of DT and DTD

The DT and DTD for all 163 catchments were used as input for geospatial analysis and pattern identification. The impact estimation of different explanatory variables and catchment properties from the CAMELS-CL data on DT and DTD using lasso regression (Tibshirani, 1996) and random forest regression (Breiman, 2001) was performed. Lasso is good to reduce multi-collinearity by putting penalties on jumping up and down regression coefficients, meanwhile, Random Forest Regression is a meta-estimator of the data set that fits a number of classifying decision trees on various sub-samples and uses averaging to improve the predictive accuracy and control over-fitting (Kramer, 2016). The random forest regression used 30% for training data, random state zero, and tree size length iteration over correlation was obtained. Other variables were included that are potentially linked with the drought recovery like the average groundwater depth (from Alvarez-Garreton et al., 2018), the average rate of sun exposition (from Farr and Kobrick, 2000), and average soil moisture capacity (from van Beek and Bierkens, 2009, all variables listed in Appendix A.5). The python package scikit-learn was used to get the best explanatory variables and random forest for the discharge, vegetation productivity, and soil moisture variables (Simpson et al., 2021).

The weight of each variable was calculated based on the residuals sum of squares from:

$$R^2 = 1 - \left(\frac{u}{v}\right) \tag{3}$$

where u is the residual sum of squares $\sum(y_{true} - y_{pred})^2$. It can be negative due to the arbitrarily worse of the model, and 1.0 is the best possible score. A filter with lasso regression was performed before RFR.

3. Results

3.1. Composite analysis

The response of each natural catchment after drought events between 1988 to 2020 is studied using a CA. Fig. 2 shows the results of CA for the "Río Cauquenes en el Arrayán" catchment (620 km^2, coordinates: 72° 30′S, 36° 6′W). The upper figure shows the average response of discharge, the central figure the kNDVI as a proxy for vegetation productivity, and the lower figure the

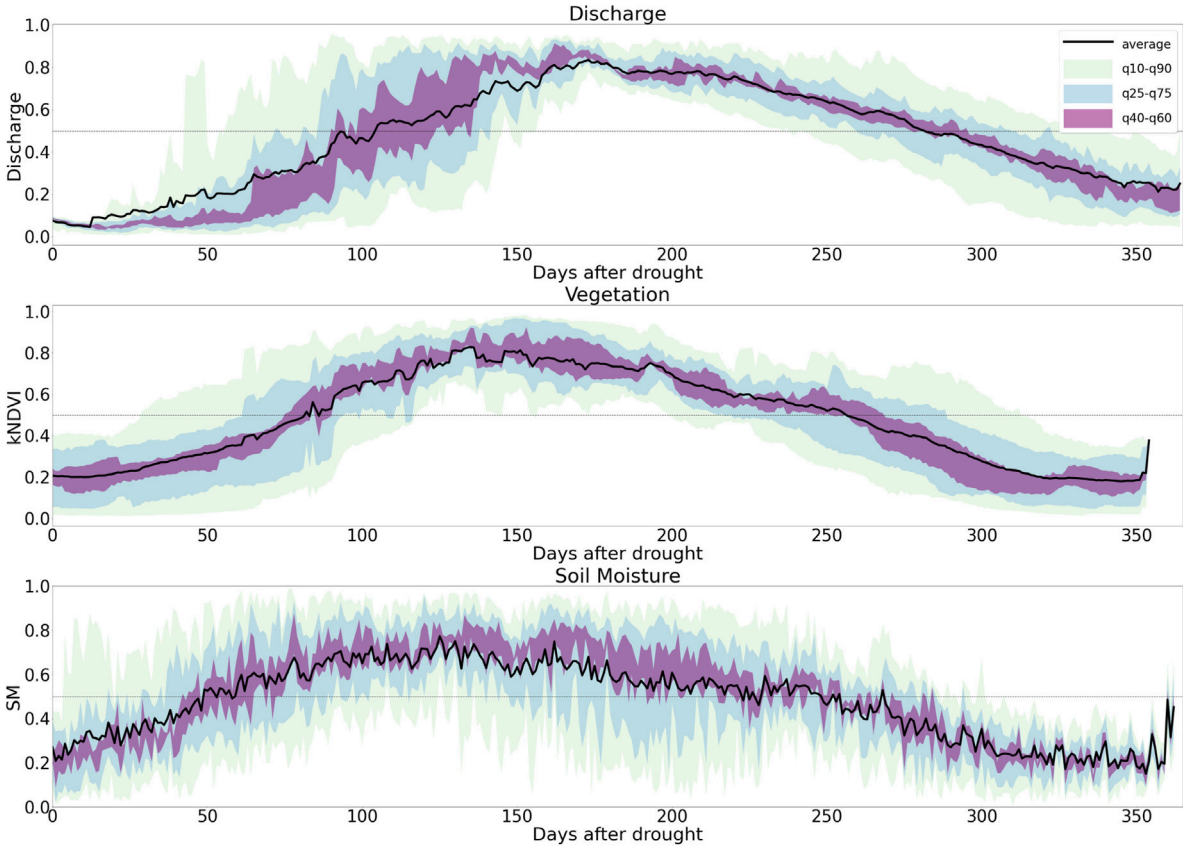

Fig. 2. Composite analysis for discharge, vegetation productivity, and soil moisture for the "Río Cauquenes en el Arrayán" catchment. In the graph the average response is shown with a black line, meanwhile, the quantiles of ensembles are distributed between 10%–90%, 25%–75%, and 40%–60%. The upper figure shows the ensembles of discharge, the middle of kNDVI, and lower soil moisture.

soil moisture. The quantiles in the graph present a skewed density distribution and correspond to the variable members between 10%–90%, 25%–75%, and 40%–60%, including the recovery threshold (0.5) which is the end of the recovery for the DT. The behavior of discharge and vegetation productivity in this catchment present a close relation in their recovery after drought events by comparing the average CA response (black line in Fig. 2). Where a fast recovery response is observed in the vegetation and a slightly slower one in the discharge. The soil moisture presents a faster recovery and may be responsible for the faster recovery of the vegetation over the discharge.

3.2. Drought recovery patterns

The spatial analysis was divided into four areas (Fig. 1) due to catchments distribution in the study area (north-Chile, central-Chile, north-Patagonia, and south-Patagonia) and bio-climatic differences (Fig. 3) .

3.2.1. Drought termination

The central-Chile area shows the main recognizable patterns visible from North to South illustrated by the changing colored circles in Fig. 3, and less clear East to West, along a gradient of precipitation and temperature. In general, dominant patterns of discharge and soil moisture, DT are visible from North to South in central Chile, meanwhile, discharge and vegetation productivity are only recognizable from East to West (Fig. 3).

The discharge (Q) (Fig. 3 left) shows a low to high recovery pattern from North to South and is, increasing until latitude −35° S. Longer discharge recovery times were found at lower latitude catchments in environments with less precipitation, higher temperatures, and mostly shrublands. While, shorter discharge recovery times were found at higher latitudes in environments with higher precipitation, lower temperatures, and high vegetation cover. After the latitude −35° S the recovery switch from high to low.

In addition, the discharge present from East to West has high to low recovery times over 300 to under 200 days, a pattern which is inverted at lower latitudes. The recovery in north Chile presents a high-to-low pattern towards the South. The north-Patagonia

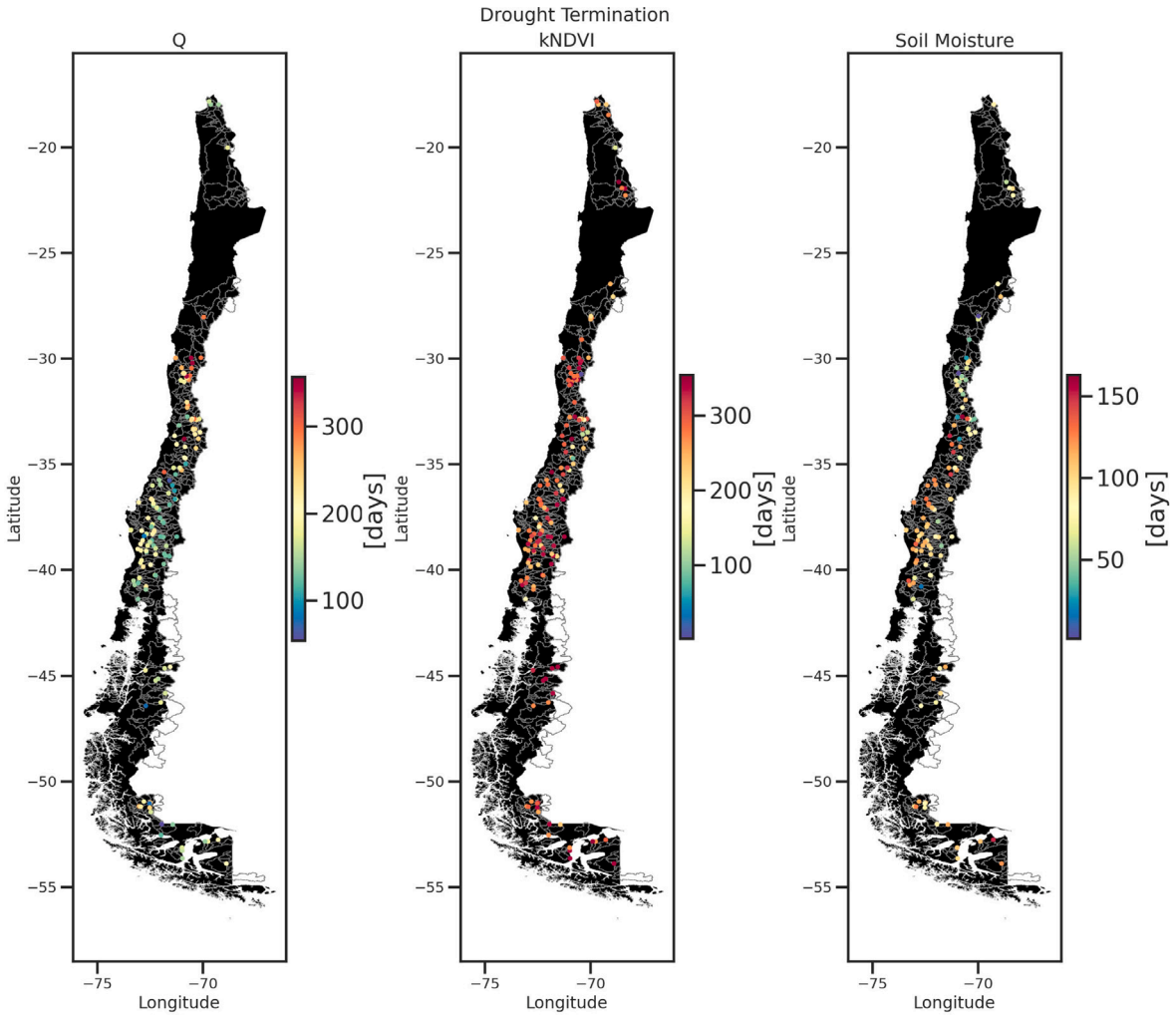

Fig. 3. Map of DT for discharge (Q), a proxy for vegetation productivity (kNDVI) and soil moisture. Each circle indicates an individual catchment and the color range indicates the time in days. (For interpretation of the references to colour in this figure legend, the reader is referred to the web version of this article.)

region presents homogeneous recovery times similar to Southcentral Chile. In south Patagonia, high to medium recovery times, between 50 to 200 days, are identified.

The vegetation shows low recovery in most of the locations without a clear pattern from North to South, however, from East to West a high-to-low recovery pattern in the North of central CL is recognized. This pattern is inverted similarly after the latitude −35° S towards the South. The north CL presents medium and high recovery times of vegetation without a clear distribution. Furthermore, the recovery in north Patagonia presents low recovery with similar behavior as Southcentral Chile. Similarly, in south Patagonia, the recovery is also low.

The recovery of soil moisture presents a high-to-low pattern from North to South in central Chile, together with a high-to-low recovery pattern from East to West in the direction of southern latitudes that is inverted after latitude −35° S. In north Chile, the recovery shows intermediate recovery times, while in north Patagonia a low recovery is present. Similar to south Patagonia.

The scale is different between variables because their responses are different, and to appreciate the spatial patterns is necessary a different scale for discharge, vegetation, and soil moisture.

3.2.2. Drought termination duration

Fig. 4 shows the results of the DTD. A dominant pattern for DTD in central Chile is visible for discharge and soil moisture from North to South. Vegetation productivity shows a less distinctive pattern (Fig. 4).

The discharge in central Chile, as for DT, presents an increased recovery time from North to South after drought events. Such a pattern is also visible from East to West with a low to high recovery pattern decreasing towards higher latitudes, and shifting after approximately −35° S. In north Chile, the discharge presents low to medium recovery times. In north Patagonia, the recovery

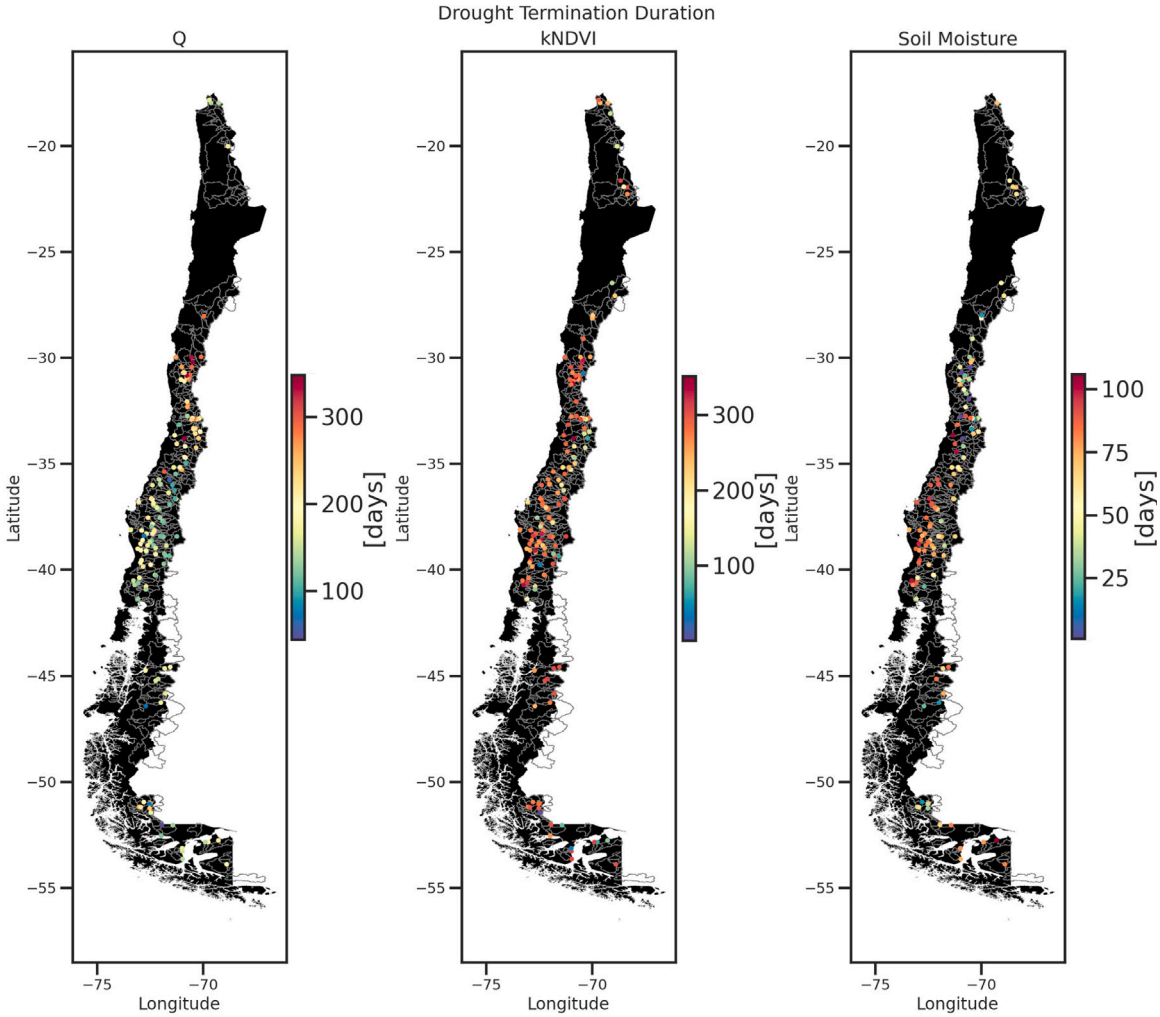

Fig. 4. Map of DTD for discharge (Q), proxy for vegetation productivity (kNDVI) and soil moisture (SM).

exhibits intermediate recovery times i.e. (150–200 days). In contrast, south-Patagonia does not show a clear pattern of recovery time.

The vegetation recovery time in central Chile does not show a clear pattern from North to South, however, from East to West, it exhibits a high to low recovery until a latitude of 35° S where the pattern is shifted towards the South. In north Chile, the recovery is low, with values close to 200 days. In addition, in northern Patagonia, the recovery is low, while in south Patagonia there is not a clear pattern with extremely high or low recovery.

The recovery of soil moisture presents a faster response compared with DT and also other variables. Particularly, central CL show high to low recovery from North to South, and a pattern from East to West with high to low recovery for all the region. The North CL evidence a slow recovery of close to 2 months. Similar to north-Patagonia which is also slow with values over 2 months, south Patagonia presents high recovery in the North and low recovery in the South (Fig. 4).

3.3. Snow accumulation and recovery

The annual streamflow in rainfall-fed catchments has a shorter hydrological memory mainly explained by the precipitation of the current year. In the case of vegetation productivity, the recovery is faster in catchments with the presence of snow, and soil moisture recovery presents a slightly higher recovery in catchments without snow accumulation. Table 1 shows the average recovery of discharge, vegetation, and soil moisture.

Table 1
Average DT and DTD in days and standard error for recovery variables.

Snow accumulation on natural catchments recovery				
Recovery	DT		DTD	
variables	Snow accum	No snow	Snow accum	No snow
Discharge	160.9 ± 7.5	113.1 ± 3.4	152.0 ± 9.3	103.7 ± 3.4
Vegetation	142.0 ± 12.6	162.8 ± 10.43	95.3 ± 9.8	95.3 ± 6.8
Soil Moisture	29.6 ± 4.4	33.8 ± 2.37	18.7 ± 2.89	28.5 ± 2.41

3.4. Recovery and Koppen climates

The discharge recovery time showed longer values in semi-arid climates, the next Mediterranean, Temperate, and Tundra climates. Our results show relatively similar recovery times for the rainy summer tundra climate of pluvial watersheds (100 days) at south-Patagonia as found by Wu et al. (2020) reporting between 60 to 390 days over three unaltered flow rainfall-driven basins under humid South Asian subtropical monsoons. The vegetation recovery showed faster average recovery in Tundra climates (2 to 5 months), followed by Mediterranean (3 to 5 months), Temperate (3 to 5 months), and Semi-arid (4 to 5.5 months). Jiao et al. (2021) also found the recovery of canopy density (4–6 months) and photosynthetically active radiation (2 to 3 months) average times to return to normal status for arid, semi-arid, semi-humid, and humid Australian ecosystems. The soil moisture recovery showed longer recovery in Mediterranean environments (4–5 weeks), followed by Temperate (3–4 weeks) and Tundra(3–4 weeks), meanwhile, Semi-arid (2–3 weeks) presented the faster recovery (Appendix 1 to 4).

Table 2
Average DT and DTD in days and the standard error for Köppen climates.

Drought recovery over Koppen climates						
Koppen	Discharge		Vegetation		Soil moisture	
climates	DT	DTD	DT	DTD	DT	DTD
Semi-Arid	192.3 ± 17.8	184.0 ± 17.3	170.4 ± 19.0	113.9 ± 14.7	21.7 ± 5.6	12.8 ± 2.4
Temperate	108.8 ± 5.4	99.0 ± 5.0	156.6 ± 18.0	92.2 ± 12.3	31.2 ± 4.5	24.8 ± 4.5
Mediterra-nean	127.7 ± 5.0	118.4 ± 5.1	147.8 ± 10.4	91.0 ± 7.2	36.8 ± 3.1	28.9 ± 2.8
Tundra	109.0 ± 6.4	100.0 ± 6.1	146.4 ± 37.9	79.3 ± 21.5	32.8 ± 4.3	25.5 ± 3.3

Table 3
R-square scores of Multiple Linear Regression (MLR) and Random Forest Regression (RFR) models. Bold indicates high significance in MLR. RFR does not provide significance.

Recovery regression models				
Recovery variables	MLR		RFR	
	DT	DTD	DT	DTD
Discharge	**0.50**	**0.47**	0.91	0.91
Vegetation	0.10	0.23	0.84	0.83
Soil Moisture	0.10	**0.38**	0.90	0.91

3.5. Multiple linear regression

The results of the MLR (Table 3) show significant values only for the discharge recovery of $R^2 = 0.5$. The vegetation productivity and soil moisture did not show significant skills to predict the DT and DTD. The explanatory variables for discharge DT and DTD are associated with precipitation, potential evapotranspiration, and baseflow, or by a combination of them with catchment characteristics related to storage and release (e.g. land use).

3.6. Random forest regression

The graphs presented in Fig. 5 show the most significant variables for the determination of DT and DTD of predicted versus observed values. In general, all the predictions have a high correlation coefficient due to the advantages of RFR for obtaining non-linear relationships. The downside of using decision trees is their tendency to overfit. We used 30% of training data, as they are highly sensitive to small changes in data.

The correlation coefficients for DT are given in Table 3 and correspond to 0.92, 0.84, and 0.89 with an RMSE coefficient of 56,57, 93,26, and 23,74 for discharge, vegetation productivity, and soil moisture, respectively. The correlation coefficients for DTD correspond to 0.92, 0.85, and 0.91 with an RMSE coefficient of 57.03, 56.50, and 19.73 for discharge, vegetation productivity, and

soil moisture, respectively. The model used 30% of the data for training and the main model features are included in the top right considering their contribution to the model and the correlation coefficient in the top left. The most efficient RFR models used 200, 200, and 500 trees for the prediction of discharge, vegetation productivity, and soil moisture of DT, meanwhile, for the DTD the number of trees corresponding to 50, 100, and 200 (Fig. 5 top left parameters).

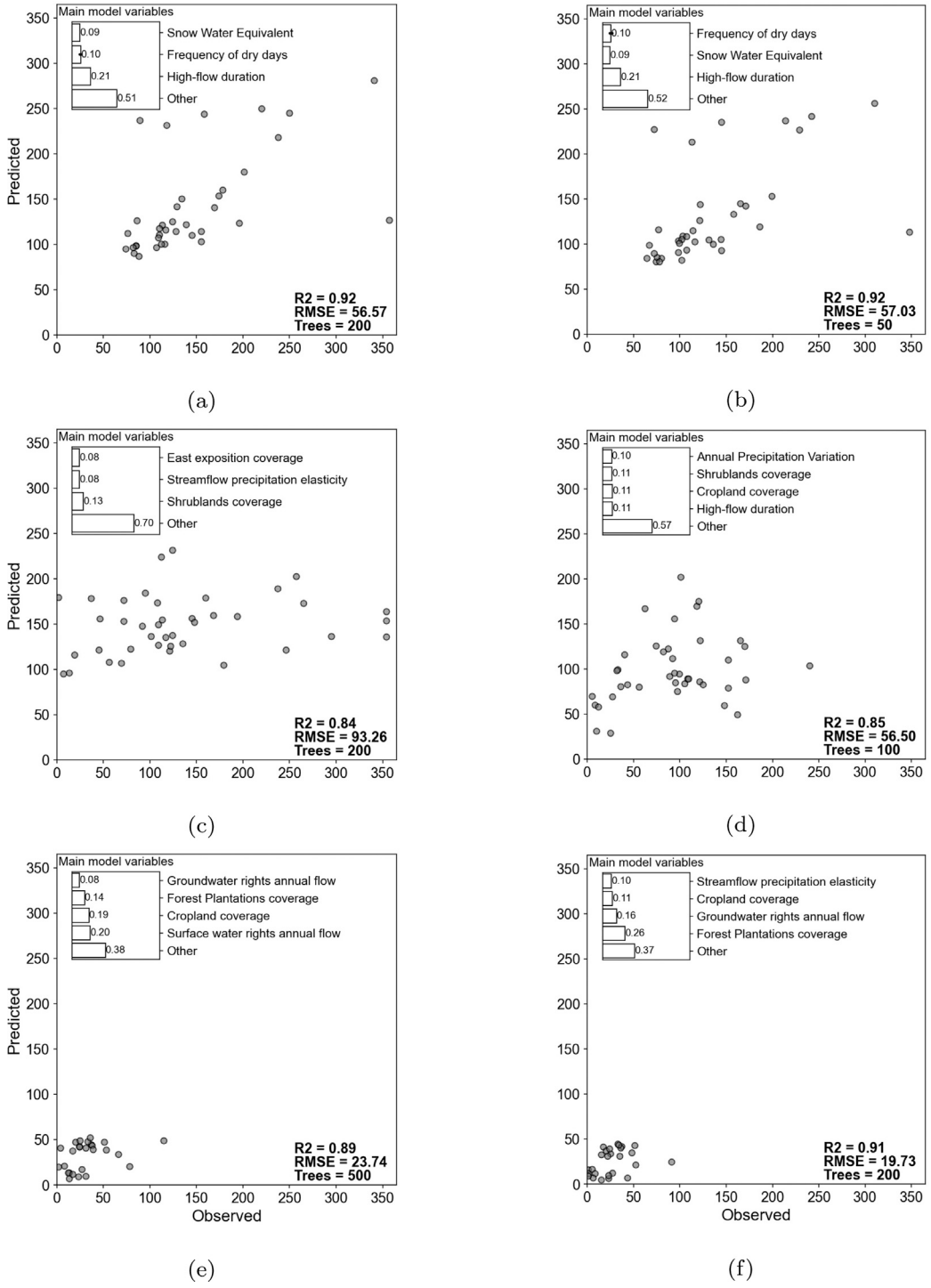

Fig. 5. Random Forest training models with 30% data used for training. (a)Discharge DT, (b)Discharge DTD, (c)Vegetation DT, (d)Vegetation DTD, (e)Soil moisture DT, (f)Soil moisture DTD.

The variables with a higher contribution to the prediction of discharge DT and DTD are presented in Fig. 5, from a to d in the upper-right corner. The most important variables for the prediction of discharge recovery are linked with precipitation, extreme discharge, and snow accumulation, meanwhile, vegetation productivity can be explained with a combination of catchment characteristics (catchment exposition ratio) associated with storage and release (shrub-land cover), and superficial water extraction. For soil moisture, the stream flow precipitation elasticity, storage–release characteristics (crop and forest cover), and water extraction (ground and superficial) are the main drivers. The ''other'' variables from the CAMELS-CL data set correspond to variables that do not contribute to the model as much as the top ones.

4. Discussion

4.1. Snow accumulation and recovery

In general, the recovery of discharge, vegetation, and soil moisture differs amongst catchments according to the presence or absence of snow. Particularly, the discharge recovery shows a slower response on catchments with snow accumulation. Correspondingly, Alvarez-Garreton et al. (2020) demonstrated that snow-dominated catchments in Chile possess a hydrological memory that results in strong correlations in stream flow generation over consecutive hydrological years.

The slow discharge recovery time of snow-fed catchments demonstrates that the recovery is hampered by snowmelt infiltration into groundwater-depleted levels reducing the river's stream flow. In addition, Alvarez-Garreton et al. (2020) demonstrated that catchments with snow accumulation (long memory) in Chile exhibit a progressive reduction in stream flow generation during the same hydrological year as catchments without snow accumulation. The multi-year drought increased the drought propagation and increased differences between rainfall-fed basins (Alvarez-Garreton et al., 2020). It is possible that the recovery of long memory basins may have been affected during a multi-year drought due to the increased frequency and intensity of hydrological drought. During this period, the flow of the stream would be reduced due to its dependence on rainfall, but mostly due to the lack of snow accumulation in the corresponding year. Other factors that may affect the recovery of the stream flow include the allocation of water rights over the rivers and groundwater in the studied basins. The replacement of native vegetation with water-demanding species such as tree exotic plantations, as well as the rapid shift in land use during the last few decades. The consequent rise in water demand for agriculture irrigation and human consumption may also have an impact (Barría et al., 2021b; Galleguillos et al., 2021).

The recovery of vegetation productivity, which is faster in catchments with snow accumulation for DT, but similar for DTD, demonstrates a different behavior. This faster recovery can be attributed to the physical properties of the soil profile (such as porosity, and resistance to penetration), which are associated with the rooting depth of the vegetation, which can reach 20 meters (*Prosopis tamarugo*), and the impact-timing of drought on the water table depth (Kannenberg et al., 2019a; Decuyper et al., 2016). In the maps presented by Schwalm et al. (2017) similar vegetation recovery for the same study area is visualized after analyzing three data sets of Gross Primary Productivity (GPP) across diverse ecosystems worldwide. In their findings, drought recovery times were strongly associated with climate and carbon cycle dynamics on a global scale. Specifically, in sparsely covered shrubland of Central Chile dominated with *Acacia caven* in a Mediterranean climate with a warm and dry season (7–8 months), the ecosystem productivity was explained mostly by rainfall frequency with a significant time lag between plant growth and precipitation events (Sepúlveda et al., 2018). This is supported by the global probability map of precipitation exceeding temperature as the main driver of tree growth for this region (Babst et al., 2019).

This can modulate the recovery since water availability acts as a crucial limit to global primary productivity, and the hydrological drought is considered the starting point of the variability in the signal. Generating global concern also, because hydrological drought is predicted to become more limiting globally (Zhou et al., 2019; Kannenberg et al., 2020). A source of uncertainty for the prediction of vegetation recovery is evidenced by Kannenberg et al. (2019b) where a decrease in tree growth can occur together with a quick recovery of GPP, showing a large legacy effect (vegetation recovery in literature) in tree rings, and growth away from the stem towards the canopy. This is due to carbon allocation shifts linked with upregulated leaf-level photosynthesis, meaning that legacy effects in GPP are much smaller than those in tree rings.

The vegetation recovery of Chile found in this study is also coherent to Ahmadi et al. (2019b) for DTD between 3–4 months (90–120 days), however, they used water use efficiency (WUE) which is a ratio between gross primary productivity (GPP) and potential-evapotranspiration (ET). The rise of WUE helps the vegetation in arid regions to reduce water loss and maintain its growth due to a series of conservative water-use strategies. With this approach in dryer regions (with high ET) is expected an increase in WUE during drought episodes, even though vegetation recovery is longer as demonstrated in this study (particularly north-central Chile) (Vicente-Serrano et al., 2013; Long et al., 2013).

Overall we can conclude that the findings from this study are in line with other studies looking at vegetation recovery using different techniques. The implications of faster recovery can imply that plants are more susceptible to future droughts, and slower recovery to a controlled acclimation response optimizes survival in the long-term (Gessler et al., 2020).

The soil moisture shows a slightly faster recovery in catchments with snow accumulation compared with rainfall-fed recovery times between 3–4 weeks. Similar recovery times for the global snow-free region of soil moisture were simulated with a land surface model (assimilating satellite microwave brightness temperature) and composite analysis of drought events by Sawada (2018). Even though their analysis did not include catchments with snow accumulation, similar hydrological processes may explain similarities in the recovery. The reductions in soil moisture after hydrological drought indicate the link with the start of agricultural drought (Leblanc et al., 2009). In this sense, the recovery of soil moisture is important for regulating vegetation growth and rainfall-runoff relationships, allowing the quick restoration of pre-conditions for the recovery (Gibson et al., 2020). Suggesting that catchments may be buffered or less impacted by drought in high-relief and well-vegetated regions (Salazar et al., 2016; Potter et al., 2015).

4.2. Climate zones and their influence on the recovery

Differences in recovery time between the various environmental conditions were also found within the studied natural catchments (Table 2). The Köppen climate classification (Table A.4) was used to demonstrate the influence of seasonality, precipitation, and temperature. Based on the ecosystem properties and approximately three decades of data, this study evidenced that most of the natural catchments in Chile experienced an average recovery post-drought with different timings for discharge (Table A.1), vegetation productivity (Table A.2) and soil moisture (Table A.3).

The discharge recovery found by Wu et al. (2020) relates the importance of precipitation in the recovery of rivers in humid South Asian subtropical monsoons with precipitation during the warm season. Consequently, the faster discharge recovery occurs in catchments with climates that present higher rainfall regimes as Temperate and Tundra environments than in Semi-Arid and Mediterranean (Xi and Yuan, 2022).

As stated previously the reduction of vegetation productivity starts after hydrological drought, which is marked by the legacy effect before the recovery (Kannenberg et al., 2020). Wu et al. (2018) stated that drought legacy effects on vegetation growth over the temperate Northern Hemisphere differ markedly between forests, shrubs, and grass across diverse bioclimatic conditions. Differences in drought legacy effects between impact plant functional groups to plant ecohydrological properties (linked to traits) can also play a role. The GPP signal can also contribute to the variability in the identification of plant recovery. Such as the plant response mechanism to carbon allocation priority, producing leaf abundance or photosynthesis instead of biomass growth in branches or stems (Kannenberg et al., 2019b).

Miranda et al. (2020) evidenced that in the Mediterranean Chilean forest the local environmental conditions which provide higher soil moisture (e.g. valley bottoms) and forest composition enhanced forest resistance/alleviation to drought. Moreover, Cartwright et al. (2020) found that areas with low soil bulk density and high soil available water capacity presented a reduced drought sensitivity (and high soil moisture recovery). However, the biome with faster soil moisture recovery corresponds to the semi-arid which presents higher bulk density and low soil water capacity (Seguel et al., 2013). The presence of higher mountains in this biome (in the Andes and coastal range) with more valley bottoms and south exposition hills (shade in the southern hemisphere) provide good conditions to retain water due to low evaporation.

4.3. Drought recovery patterns

Spatio-temporal recovery of river discharge, vegetation productivity, and soil moisture is critical to investigate in regions without enough measurements and under increasing environmental pressure due to climate change and human activity. As proven by this study, collecting discharge data is important for understanding the processes in the catchment. The method proposed in this study provides a comprehensive tool to assess regional drought vulnerability, which is important for the effective basin-scale management of water resources and ecosystems.

In central Chile river discharge patterns exhibit a reduction in the recovery times from north to south. This recovery pattern follows Masiokas et al. (2020) regional stream flow classification patterns for south America. They estimated the north of central Chile, presented the lowest recovery times, and the lowest discharge during the rainy season of rivers. Followed by an early summer single discharge peak that largely reflects the winter snow accumulation levels. The recovery gradient from west to east is associated with the influence of winter orographic precipitation in the lower catchments, between the coastal mountains and the valley, which enhanced the recovery (Viale et al., 2019). Southern central Chile shows an inverted pattern compared to the north. A gradient of low recovery near the latitude of 35° S is found and this becomes slightly higher towards the south. Masiokas et al. (2020) described this group of rivers as part of the lower Andes (smaller mountain range height) with wetter conditions than the north. In this region, stream flows present a winter peak largely due to precipitation and in some cases a second spring peak due to snow melt. The decreased recovery pattern from east to west is explained by the higher influence of precipitation, reaching catchments located in the lower Andes (further than in the north), and the addition of snowmelt discharge on the east (Garreaud et al., 2020). The patterns in north Patagonia are also described by Masiokas et al. (2020) as a single spring peak discharge due to snow-melt with milder climatic conditions due to the low elevation of the Andes, and winter liquid precipitation.

The vegetation recovery Spatio-temporal patterns show longer recovery in densely vegetated areas of south-central Chile, and faster recovery on semi-arid shrublands of the high Andes in central Chile. The maps developed by Schwalm et al. (2017) showed long recovery times in highly vegetated mountains of southern Andes with values between 6 to 12 months too, and recovery times of 3 to 6 months for the rest of the territory. However, the catchments placed in the arid and semi-arid high Andes of this study evidenced faster recovery (4 months) between the −30° S to −35° S degrees, and the rest of central Chile presented values over 6 months. DeChant and Moradkhani (2015) also found that semi-arid vegetation recovers quickly in the upper Colorado River basin due to loss of sensitivity to initial conditions of soil water storage after droughts in the mountainous northeastern region of the semi-arid upper Colorado river basin (US). Contrary, in their low-lying arid southern and western regions the recovery was slow after drought events. Cartwright et al. (2020) showed at a regional scale that ecosystems with a drier climate and lower biomass (shrub-steppe) showed greater drought sensitivity (greenness reduction relative to baseline soil moisture) than conifer forests in the Pacific Northwest, USA. In their study drought sensitivity was generally greater in zones with high elevation, drier climate, and greater soil bulk density. Identifying variability in drought sensitivity within biomes and within ecosystems, mediated by landscape topography, climate, and soil characteristics. Zhang et al. (2021) found diverse post-drought recovery trajectories for different biomes, with forest ecosystems showing a longer recovery time compared with shrublands and grasslands. Jiao et al. (2021) evidenced for Australian ecosystems, that forests and savanna required the longest recovery times for “press drought” (> 3 months but not extreme drought),

while grasslands were the slowest to recover for "press drought" (> 3 months extreme drought). This may explain the differences between patterns of recovery in catchments close to each other with these characteristics in central Chile and different vegetation compositions (e.g. between −39° S and −38° S). Even though, DeChant and Moradkhani (2015) reported that the vegetation drought recovery rate seems to be more related to specific locations than drought intensity. This can suggest that intensity variation due to propagation is less relevant for vegetation recovery than the local characteristics of the site, which are further evaluated using random forest regression. Where site exposition, land use, surface water rights, and annual precipitation variation are the main relevant factors. Also, most of the catchments of this region have experienced significant land cover change during the last hundred years (Lara et al., 2012). Shrub lands in northern Chile have been transformed into avocado plantations over the last 10 years, while native forest in central Chile has been converted into productive plantations over the last 30 years native forest was converted into productive plantations. Furthermore, deforestation of agricultural lands took place all over central Chile in the last 100 years (Lara et al., 2012). This adds a third component to plant recovery, which is the physiological response of native and exotic species to droughts and their recovery time at the study site. Mediterranean species possess special adaptations to a drought that may influence the recovery as the storage of soluble carbohydrates during summer (Martínez-Vilalta et al., 2016). However, is not clear yet if this helps them to accelerate or extend the recovery as part of the legacy effects of drought impact. Studies carried by Venegas-González et al. (2018), Matskovsky et al. (2021) reported that the Mediterranean endangered and endemic forest of *Nothofagus macrocarpa* and *Austrocedrus chilensis* in central Chile presented an increased declination of radial growth in the last decades due to drought conditions.

The spatial distribution of soil moisture recovery presents patterns that may be related to discharge recovery. DeChant and Moradkhani (2015) also demonstrated the difference between drought recovery time and rate of recovery. Since the drought recovery time is highly dependent on initial conditions of soil moisture, and this value varies strongly temporally, they reported that this variable is linked to the discharge recovery in terms of their geographical patterns. In this sense, soil moisture and discharge recovery presented an opposite gradient behavior in this study. This is, at a faster discharge recovery towards the south of central Chile there is a slow soil moisture recovery. The patterns can be also observed from east to west, which tells that as rivers recover faster the soil moisture recovers slowly. The reason for this pattern could be the preferential transport of water to the rivers when they are recovering and the consequent diminution of the soil moisture in the first 5–10 cm. Also, surface run-off with high rainfall intensity could be attributed to low infiltration in the first layers of soil, improving only the discharge recovery (Woolhiser and Goodrich, 1988; Molina et al., 2007).

4.4. Random forest regression

The predictors of DT and DTD (Fig. 4) are connected to diverse hydrological processes with different contribution proportions to the model. The processes linked with the discharge recovery model predictors are related to water provisions such as precipitation, stream flow extremes, and snow accumulation. In this sense, when a precipitation event begins, it is also where and when drought starts the recovery with a lag until surface runoff reaches the outlet. Moreover, the first rainy events after a dry period can provide extreme flows, or even flash flows, due to the effect of water repellency influenced by antecedent soil water content, hydraulic conductivity, and precipitation intensity (Cerda et al., 1998). Snow accumulation is particularly relevant for watersheds with high elevations and low elasticity of stream flow to precipitation and temperature changes in Chile (Barrera et al., 2020). Also, snow accounts for the storage of water, provisioning water during dry periods, and even in dry periods, providing water to the stream flow and groundwater. However, in the short term, higher snowmelt rates may help the recovery temporarily due to higher temperatures in Chile (Garreaud et al., 2020). In the long term, this may induce snow drought due to early snow melt in combination with no recharge due to precipitation deficit (Van Loon, 2015).

The vegetation recovery RFR model presents predictors that are connected to precipitation behavior together with water storage and release characteristics by the land cover (shrub land cover). The inclusion of the annual precipitation variation responds to the influence of El-Niño-Southern-Oscillation and the reduction of precipitation due to the Southern Blob in the last years (Garreaud et al., 2021). The storage and release are mainly influenced by plants' adaptation to efficient use of water (Martínez-Vilalta et al., 2016), the influence of climate change on vegetation relocation distribution patterns (Batllori et al., 2020), soil storage properties (Galleguillos et al., 2021) and land cover change (Alvarez-Garreton et al., 2019). The superficial water extraction as an explanatory variable relates the recovery with the private water rights system in Chile. Which is not limited by catchments' water provision capacity (Barría et al., 2021b). Even though there is an extreme reduction in river stream flow due to the multi-year drought during the last decade for many of them (Alvarez-Garreton et al., 2020). The relevance of orographic precipitation across the coastal mountain range, which is exacerbated in mesic locations, is demonstrated by east exposition as a predictor (Cazorla et al., 2022; Viale et al., 2019).

The explanatory variables of the soil moisture recovery model, such as superficial-ground water extraction and land cover, evidence that water management at a catchment scale is very relevant for this region (Barría et al., 2021a). In this regard, the assessment of drought termination and resilience may improve planning and resource management at the catchment scale under future climate change droughts (Van Loon et al., 2016). At the moment the water rights market presents over-allocation and may generate an even more extreme situation considering the weather predictions (Barría et al., 2021b; Gibson et al., 2020). Climate change projections include precipitation reductions and higher temperatures that may increase evaporation and reduce soil moisture which will account for the increase in hydrological droughts (Wada et al., 2013). Similar projections show an increase in drought areas for Europe up to 40% with a consequent exacerbation of soil moisture droughts (Samaniego et al., 2018).

5. Conclusion

This study investigated the impacts of multi-year droughts in Chile and analyzed for 163 catchments the drought duration and recovery time related to environmental conditions. It demonstrates that the recovery of discharge, vegetation productivity, and soil moisture after a hydrological drought can be explained by local catchment properties and characteristics. The outcome of this study is a contribution to disentangling the connection of environmental conditions (vegetation and soil moisture) and discharge to assess the drought vulnerability of catchments. The recovery analysis over different climate zones also contributes to the supply of quantitative thresholds to improve the modeling of ecosystem dynamics post-drought.

Snow accumulation influences the recovery of natural catchments compared to rain-fed basins. The decrease in discharge recovery due to snow melt infiltration into groundwater levels reduces the river's stream flow. The vegetation recovery evidences faster recovery in watersheds with snow accumulation due to the constant water provision through the groundwater profile. Helping with water provision to species adapted to dry conditions and with deeper roots. The soil moisture recovery presents higher recovery in basins with snow consequently due to the longer provision of water.

Environments dominated by shrublands, with less precipitation and higher temperatures present longer discharge recovery, while in higher latitudes, with increasing precipitation and lower temperatures the recovery times are shorter under higher vegetation cover. The patterns of vegetation show longer recovery in densely vegetated areas of south-central Chile, and faster recovery in semi-arid shrublands of the high Andes in central Chile. The spatial distribution of soil moisture recovery presents patterns that connect them with discharge recovery. This might be explained by the preferential transport towards streams, and the increasing surface run-off due to high rainfall intensity with low infiltration of the first layers of soil.

The recovery of discharge is better explained by precipitation, extreme discharge, and snow accumulation, meanwhile, vegetation productivity by a combination of catchment characteristics (catchment exposition ratio) associated with storage and release (shrubland cover), and superficial water extraction. The soil moisture main predictors correspond to stream flow precipitation elasticity, storage–release characteristics, and ground-superficial water extraction.

This study shows for the first time the discharge recovery for different environments at the catchment scale, along with the recovery of vegetation productivity and soil moisture. This is useful for the identification of drought vulnerability for managing water resources and ecosystems, helping to predict drought recovery periods in regions with scarce observations.

CRediT authorship contribution statement

Jorge Vega-Briones: Data curation, Formal analysis, Writing – original draft, Visualization, Investigation. **Steven de Jong:** Conceptualization, Methodology, Reviewing and editing. **Mauricio Galleguillos:** Conceptualization, Reviewing and editing. **Niko Wanders:** Conceptualization, Methodology, Supervision, Writing – review & editing, Project administration.

Declaration of competing interest

The authors declare that they have no known competing financial interests or personal relationships that could have appeared to influence the work reported in this paper.

Data availability

CAMELS-CL, CCI Soil Moisture and MODIS are open source data sets.

Acknowledgments

Jorge Vega-Briones reports financial support by ANID PhD 72210588.

Appendix. Tables

See Tables A.1–A.6.

Table A.1
Recovery of discharge for different climates.

Discharge DT and DTD				
Koppen	DT		DTD	
climates	Snow	NoSnow	Snow	NoSnow
Mediterranean climate of winter rain (Csb)	122.8	114.9	113.4	105.4
Mediterranean climate with high altitude winter rain (Csb(h))	169.7	–	160.9	–
Semi-arid climate with winter rain (BSk(s))	209.6	–	201.2	–
Tundra climate (ET)	–	116.3	–	106.3
Summer rainy tundra climate (ET(w))	–	103.5	–	95.2
Mediterranean climate with winter rain and coastal influence (Csb(i))	–	137.0	–	125.3
winter rain cold Mediterranean climate (Csc)	–	124.8	–	117.0
Semi-arid climate (BSk)	–	84.3	–	76.3
Rainy temperate climate (Cfb)	–	97.3	–	88.0
Rainy temperate climate with mild summer dryness (Cfb(s))	–	109.5	–	99.4
Rainy temperate climate with slight summer dryness and coastal influence (Cfb(s)(i))	–	97.5	–	88.0
Rainy temperate climate and coastal influence (Cfb(i))	–	89.0	–	80.0
Cold rainy temperate climate (Cfc)	–	142.0	–	132.3

Table A.2
Recovery of vegetation productivity for different climates.

Vegetation DT and DTD				
Koppen	DT		DTD	
climates	Snow	NoSnow	Snow	NoSnow
Mediterranean climate of winter rain (Csb)	132.9	174.3	82.5	111.9
Mediterranean climate with high altitude winter rain (Csb(h))	92.4	–	58.5	–
Semi-arid climate (BSk)	72.0	138.6	7	49.6
Semi-arid climate with winter rain (BSk(s))	176.5	–	128.6	–
Tundra climate (ET)	–	192.2	–	90.7
Summer rainy tundra climate (ET(w))	–	115.8	–	71.6
Mediterranean climate with winter rain and coastal influence (Csb(i))	–	69.3	–	57.0
winter rain cold Mediterranean climate (Csc)	–	188.8	–	91.2
Semi-arid climate with summer rain (BSk(w))	–	187.6	–	89.6
Rainy temperate climate (Cfb)	–	214.6	–	103.0
Rainy temperate climate with mild summer dryness (Cfb(s))	–	147.5	–	80.2
Rainy temperate climate with slight summer dryness and coastal influence (Cfb(s)(i))	–	193.5	–	179.0
Rainy temperate climate and coastal influence (Cfb(i))	–	28.0	–	18.0
Cold rainy temperate climate (Cfc)	–	107.6	–	102.0

Table A.3
Recovery of soil moisture for different climates.

Soil moisture DT and DTD				
Koppen	DT		DTD	
climates	Snow	NoSnow	Snow	NoSnow
Mediterranean climate of winter rain (Csb)	132.9	174.3	82.5	111.9
Mediterranean climate with high altitude winter rain (Csb(h))	92.4	–	58.5	–
Semi-arid climate (BSk)	72.0	138.6	7	49.6
Semi-arid climate with winter rain (BSk(s))	176.5	–	128.6	–
Tundra climate (ET)	–	37.0	–	27.75
Summer rainy tundra climate (ET(w))	–	24.5	–	21.0

(*continued on next page*)

Table A.3 (*continued*).

Soil moisture DT and DTD				
Koppen	DT		DTD	
climates	Snow	NoSnow	Snow	NoSnow
Mediterranean climate with winter rain and coastal influence (Csb(i))	–	44.0	–	39.0
winter rain cold Mediterranean climate (Csc)	–	42.8	–	29.0
Semi-arid climate with summer rain (BSk(w))	–	14.3	–	14.0
Rainy temperate climate (Cfb)	–	25.2	–	18.0
Rainy temperate climate with mild summer dryness (Cfb(s))	–	27.2	–	25.8
Rainy temperate climate with slight summer dryness and coastal influence (Cfb(s)(i))	–	63.0	–	56.6
Rainy temperate climate and coastal influence (Cfb(i))	–	11.0	–	6.0
Cold rainy temperate climate (Cfc)	–	43.5	–	10.5

Table A.4
Recovery of DT and DTD for different climates.

Recovery variables						
Koppen	Discharge		Vegetation		Soil moisture	
climates	DT	DTD	DT	DTD	DT	DTD
BSk	84.3	76.3	122.0	39.0	28.6	21.0
BSk(s)	209.6	201.2	176.56	128.6	21.8	11.6
BSk(s)(i)	205.0	197.0	160.0	119.0	–	–
BSk(w)	–	–	187.6	89.6	14.3	14.0
Cfb	97.3	88.0	214.6	103.0	25.2	18.0
Cfb(i)	89.0	80.0	28.0	18.0	11.0	6.0
Cfb(s)	109.5	99.4	147.5	80.2	27.2	25.8
Cfb(s)(i)	97.5	88.0	193.5	179.0	63.0	56.5
Cfc	142.0	132.3	107.6	102.0	43,5	10,5
Csb	118.4	108.9	155.7	98.7	39,3	31.4
Csb(h)	169.7	160.9	92.4	58.5	12,4	8.0
Csb(i)	137.0	125.3	69.3	57.0	44,0	39.0
Csc	124.9	117.0	188.9	91.2	42,8	29.0
ET	116.3	106.3	192.2	90.7	37.0	27.7
ET(w)	103.5	95.2	115.8	71.6	24.5	21.0

Table A.5
CAMELS and additional variables for models 1.

soil moisture capacity	avg exposition
avg groundwater depth	catchment area
gauge elevation	mean elevation
median elevation	max elevation
min elevation	mean slope
geological 1st class fraction	geological 2nd class fraction
carbonate sedimentary rocks fraction	cropland coverage fraction
natural broadleaf forest fraction	forest plantation coverage fraction
grassland coverage fraction	shrubland coverage fraction
wetlands coverage fraction	impervious areas fraction
barrenlands coverage fraction	snow and ice coverage fraction
glaciers coverage fraction	forest plantation index
forests covered fraction	dominant land cover fraction
missing land cover fraction	mean precipitation cr2met
mean precipitation chirps	mean precipitation mswep
mean potential evapotranspiration	aridity index
aridity chirps	aridity mswep
precipitation seasonality and timing cr2met	precipitation seasonality and timing chirps
precipitation seasonality and timing mswep	snow precipitation fraction cr2met
snow precipitation fraction chirps	snow precipitation fraction mswep
high-precipitation days frequency cr2met	high-precipitation days frequency chirps
high-precipitation days frequency mswep	average high-precipitation duration cr2met
average high-precipitation duration chirps	average high-precipitation duration mswep

Table A.6
CAMELS and additional variables for models 2.

high-precipitation season cr2met	high-precipitation season mswep
dry days frequency cr2met	dry days frequency chirps
dry days frequency mswep	average dry periods duration cr2met
average dry periods duration chirps	average dry periods mswep
dry period season cr2met	dry period season mswep
annual precipitation variation	mean discharge
runoff ratio cr2met	runoff ratio chirps
runoff ratio mswep	streamflow precipitation elasticity cr2met
streamflow precipitation elasticity chirps	streamflow precipitation elasticity mswep
flow duration curve duration	baseflow index
mean half-flow date	95% flow quantile
5% flow quantile	frequency of high-flow days
high-flow duration	low-flow duration
low discharge duration	days without discharge
swe_ratio	Number of surface water rights
surface water rights flow	surface water rights annual flow
groundwater rights annual flow	

References

AghaKouchak, A., Mirchi, A., Madani, K., Di Baldassarre, G., Nazemi, A., Alborzi, A., Anjileli, H., Azarderakhsh, M., Chiang, F., Hassanzadeh, E., Huning, L.S., Mallakpour, I., Martinez, A., Mazdiyasni, O., Moftakhari, H., Norouzi, H., Sadegh, M., Sadeqi, D., Van Loon, A.F., Wanders, N., 2021. Anthropogenic drought: Definition, challenges, and opportunities. Rev. Geophys. 59 (2), 1–23. http://dx.doi.org/10.1029/2019RG000683.

Ahmadi, B., Ahmadalipour, A., Moradkhani, H., 2019a. Hydrological drought persistence and recovery over the CONUS: A multi-stage framework considering water quantity and quality. Water Res. 150, 97–110. http://dx.doi.org/10.1016/j.watres.2018.11.052.

Ahmadi, B., Ahmadalipour, A., Tootle, G., Moradkhani, H., 2019b. Remote sensing of water use efficiency and terrestrial drought recovery across the Contiguous United States. Remote Sens. 11 (6), http://dx.doi.org/10.3390/RS11060731.

Alvarez-Garreton, C., Boisier, J.P., Garreaud, R., Seibert, J., Vis, M., 2020. Progressive water deficits during multi-year droughts in central-south Chile. Hydrol. Earth Syst. Sci. Discuss. (June), 1–23. http://dx.doi.org/10.5194/hess-2020-249.

Alvarez-Garreton, C., Lara, A., Boisier, J.P., Galleguillos, M., 2019. The impacts of native forests and forest plantations on water supply in Chile. Forests 10 (6), 1–18. http://dx.doi.org/10.3390/f10060473.

Alvarez-Garreton, C., Mendoza, P.A., Pablo Boisier, J., Addor, N., Galleguillos, M., Zambrano-Bigiarini, M., Lara, A., Puelma, C., Cortes, G., Garreaud, R., McPhee, J., Ayala, A., 2018. The CAMELS-CL dataset: Catchment attributes and meteorology for large sample studies-Chile dataset. Hydrol. Earth Syst. Sci. 22 (11), 5817–5846. http://dx.doi.org/10.5194/hess-22-5817-2018.

Babst, F., Bouriaud, O., Poulter, B., Trouet, V., Girardin, M.P., Frank, D.C., 2019. Twentieth century redistribution in climatic drivers of global tree growth. Sci. Adv. 5 (1), 1–10. http://dx.doi.org/10.1126/sciadv.aat4313.

Barrera, C., Núñez Cobo, J., Souvignet, M., Oyarzún, J., Oyarzún, R., 2020. Streamflow elasticity, in a context of climate change, in arid Andean watersheds of north-central Chile. Hydrol. Sci. J. 65 (10), 1707–1719. http://dx.doi.org/10.1080/02626667.2020.1770764.

Barría, P., Chadwick, C., Ocampo-Melgar, M., Garreaud, R., Díaz-Vasconcellos, R., Poblete, D., Rubio-Álvarez, E., Poblete-Caballero, D., 2021a. Water management or megadrought: What caused the Chilean Aculeo Lake drying? Reg. Environ. Change 21 (1), http://dx.doi.org/10.1007/s10113-021-01750-w.

Barría, P., Sandoval, I.B., Guzman, C., Chadwick, C., Alvarez-Garreton, C., Díaz-Vasconcellos, R., Ocampo-Melgar, R., 2021b. Water allocation under climate change: A diagnosis of the Chilean system. Elementa 9 (1), 1–20. http://dx.doi.org/10.1525/elementa.2020.00131.

Batllori, E., Lloret, F., Aakala, T., Anderegg, W.R., Aynekulu, E., Bendixsen, D.P., Bentouati, A., Bigler, C., Burk, C.J., Camarero, J.J., Colangelo, M., Coop, J.D., Fensham, R., Floyd, M.L., Galiano, L., Ganey, J.L., Gonzalez, P., Jacobsen, A.L., Kane, J.M., Kitzberger, T., Linares, J.C., Marchetti, S.B., Matusick, G., Michaelia, M., Navarro-Cerrillo, R.M., Pratt, R.B., Redmond, M.D., Rigling, A., Ripullone, F., Sangüesa-Barreda, G., Sasal, Y., Saura-Mas, S., Suarez, M.L., Veblen, T.T., Vilà-Cabrera, A., Vincke, C., Zeeman, B., 2020. Forest and woodland replacement patterns following drought-related mortality. Proc. Natl. Acad. Sci. USA 117 (47), 29720–29729. http://dx.doi.org/10.1073/pnas.2002314117.

Beer, C., Reichstein, M., Tomelleri, E., Ciais, P., Jung, M., Carvalhais, N., Rödenbeck, C., Arain, M.A., Baldocchi, D., 2010. Covariation with climate. Science 329 (August), 834–839.

Boisier, J.P., Rondanelli, R., Garreaud, R.D., Muñoz, F., 2016. Anthropogenic and natural contributions to the Southeast Pacific precipitation decline and recent megadrought in central Chile. Geophys. Res. Lett. 43 (1), 413–421. http://dx.doi.org/10.1002/2015GL067265.

Bozkurt, D., Rojas, M., Boisier, J.P., Valdivieso, J., 2017. Climate change impacts on hydroclimatic regimes and extremes over Andean basins in central Chile. Hydrol. Earth Syst. Sci. Discuss. (January), 1–29. http://dx.doi.org/10.5194/hess-2016-690.

Breiman, L., 2001. Random Forest, Vol. 45. Kluwer Academic Publishers, pp. 5–32, Machine Learning.

Camps-Valls, G., Campos-Taberner, M., Moreno-Martinez, A., Walther, S., Duveiller, G., Cescatti, A., Mahecha, M.D., Muñoz-Marí, J., García-Haro, F.J., Guanter, L., Jung, M., Gamon, J.A., Reichstein, M., Running, S.W., 2021. A unified vegetation index for quantifying the terrestrial biosphere. Sci. Adv. 7 (9), 1–11. http://dx.doi.org/10.1126/sciadv.abc7447.

Cartwright, J.M., Littlefield, C.E., Michalak, J.L., Lawler, J.J., Dobrowski, S.Z., 2020. Topographic, soil, and climate drivers of drought sensitivity in forests and shrublands of the Pacific Northwest, USA. Sci. Rep. 10 (1), 1–13. http://dx.doi.org/10.1038/s41598-020-75273-5.

Cazorla, M.d.C., Gallardo, L., Jiménez, R., 2022. The complex Andes region needs improved efforts to face climate extremes. Elementa: Sci. Anthropocene 1–10.

Cerda, A., Schnabel, S., Ceballos, A., Gomez-Amelia, D., 1998. Soil hydrological response under simulated rainfall in the Dehesa land system (Extremadura, SW Spain) under drought conditions. Earth Surf. Processes Landforms 23 (3), 195–209. http://dx.doi.org/10.1002/(SICI)1096-9837(199803)23:3<195::AID-ESP830>3.0.CO;2-I.

Chree, C., 1913. Some phenomena of sunspots and of terrestrial magnetism at Kew Observatory. Philosophical Transactions of the Royal Society of London. Philos. Trans. R. Soc. Lond. 212 (Series A, Containing Papers of a Mathematical or Physical Character), 75–116.

Chree, C., 1914. Some phenomena of sunspots and of terrestrial magnetism. Part II. Philos. Trans. R. Soc. Lond. Ser. A 213 (Series A, Containing Papers of a Mathematical or Physical Character), 245–277.

CONAF, 2018. Catastro de Usos de Suelo y Vegetacion. Corporacion Nacional Forestal (Chile).

DeChant, C.M., Moradkhani, H., 2015. Analyzing the sensitivity of drought recovery forecasts to land surface initial conditions. J. Hydrol. 526, 89–100. http://dx.doi.org/10.1016/j.jhydrol.2014.10.021.

Decuyper, M., Chávez, R.O., Copini, P., Sass-Klaassen, U., 2016. A multi-scale approach to assess the effect of groundwater extraction on Prosopis tamarugo in the Atacama Desert. J. Arid Environ. 131, 25–34. http://dx.doi.org/10.1016/j.jaridenv.2016.03.014.

Dekking, F., Kraaikamp, C., Lopuhaa, H., Meester, L., 2005. A Modern Introduction to Probability and Statistics. Understanding Why and How. In: Springer Texts in Statistics, http://dx.doi.org/10.2307/2983537.

Didan, K., Munoz, A.B., Solano, R., Huete, A., 2015. MODIS Vegetation Index User 's Guide (Collection 6). Univ. Ariz. 2015 (May), 31.

ESA, 2021. CCI-SoilMoisture. URL https://esa-soilmoisture-cci.org/node/93.

Farr, T.G., Kobrick, M., 2000. Shuttle radar topography mission produces a wealth of data. Eos 81 (48), 583–585. http://dx.doi.org/10.1029/EO081i048p00583.

Fernández, B., Gironás, J., 2021. Water Resources of Chile, Vol. 8. p. 433, URL http://link.springer.com/10.1007/978-3-030-56901-3.

Galleguillos, M., Gimeno, F., Puelma, C., Zambrano-Bigiarini, M., Lara, A., Rojas, M., 2021. Disentangling the effect of future land use strategies and climate change on streamflow in a Mediterranean catchment dominated by tree plantations. J. Hydrol. 595 (February), http://dx.doi.org/10.1016/j.jhydrol.2021.126047.

Garreaud, R.D., Alvarez-Garreton, C., Barichivich, J., Pablo Boisier, J., Christie, D., Galleguillos, M., LeQuesne, C., McPhee, J., Zambrano-Bigiarini, M., 2017. The 2010–2015 megadrought in central Chile: Impacts on regional hydroclimate and vegetation. Hydrol. Earth Syst. Sci. 21 (12), 6307–6327. http://dx.doi.org/10.5194/hess-21-6307-2017.

Garreaud, R.D., Boisier, J.P., Rondanelli, R., Montecinos, A., Sepúlveda, H.H., Veloso-Aguila, D., 2020. The Central Chile Mega Drought (2010–2018): A climate dynamics perspective. Int. J. Climatol. 40 (1), 421–439. http://dx.doi.org/10.1002/joc.6219.

Garreaud, R.D., Clem, K., Vicencio, J.M., 2021. The south Pacific pressure trend dipole and the Southern Blob. J. Clim. 1–54. http://dx.doi.org/10.1175/jcli-d-20-0886.1.

Gazol, A., Camarero, J.J., Vicente-Serrano, S.M., Sánchez-Salguero, R., Gutiérrez, E., de Luis, M., Sangüesa-Barreda, G., Novak, K., Rozas, V., Tíscar, P.A., Linares, J.C., Martín-Hernández, N., Martínez del Castillo, E., Ribas, M., García-González, I., Silla, F., Camisón, A., Génova, M., Olano, J.M., Longares, L.A., Hevia, A., Tomás-Burguera, M., Galván, J.D., 2018. Forest resilience to drought varies across biomes. Global Change Biol. 24 (5), 2143–2158. http://dx.doi.org/10.1111/gcb.14082.

Gessler, A., Bottero, A., Marshall, J., Arend, M., 2020. The way back: Recovery of trees from drought and its implication for acclimation. New Phytol. 228 (6), 1704–1709. http://dx.doi.org/10.1111/nph.16703.

Gibson, A.J., Verdon-Kidd, D.C., Hancock, G.R., Willgoose, G., 2020. Catchment-scale drought: Capturing the whole drought cycle using multiple indicators. Hydrol. Earth Syst. Sci. 24 (4), 1985–2002. http://dx.doi.org/10.5194/hess-24-1985-2020.

González, M.E., Gómez-González, S., Lara, A., Garreaud, R., Díaz-Hormazábal, I., 2018. The 2010–2015 Megadrought and its influence on the fire regime in central and south-central Chile. Ecosphere 9 (8), http://dx.doi.org/10.1002/ecs2.2300.

Heimann, M., Reichstein, M., 2008. Terrestrial ecosystem carbon dynamics and climate feedbacks. Nature 451 (7176), 289–292. http://dx.doi.org/10.1038/nature06591.

Jiao, T., Williams, C.A., De Kauwe, M.G., Schwalm, C.R., Medlyn, B.E., 2021. Patterns of post-drought recovery are strongly influenced by drought duration, frequency, post-drought wetness, and bioclimatic setting. Global Change Biol. 27 (19), 4630–4643. http://dx.doi.org/10.1111/gcb.15788.

Justice, C.O., Townshend, J.R., Vermote, E.F., Masuoka, E., Wolfe, R.E., Saleous, N., Roy, D.P., Morisette, J.T., 2002. An overview of MODIS Land data processing and product status. Remote Sens. Environ. 83 (1–2), 3–15. http://dx.doi.org/10.1016/S0034-4257(02)00084-6.

Kannenberg, S.A., Maxwell, J.T., Pederson, N., D'Orangeville, L., Ficklin, D.L., Phillips, R.P., 2019a. Drought legacies are dependent on water table depth, wood anatomy and drought timing across the eastern US. Ecol. Lett. 22 (1), 119–127. http://dx.doi.org/10.1111/ele.13173.

Kannenberg, S.A., Novick, K.A., Phillips, R.P., 2019b. Anisohydric behavior linked to persistent hydraulic damage and delayed drought recovery across seven North American tree species. New Phytol. 222 (4), 1862–1872. http://dx.doi.org/10.1111/nph.15699.

Kannenberg, S.A., Schwalm, C.R., Anderegg, W.R., 2020. Ghosts of the past: How drought legacy effects shape forest functioning and carbon cycling. Ecol. Lett. 23 (5), 891–901. http://dx.doi.org/10.1111/ele.13485.

Kramer, O., 2016. Machine Learning for Evolution Strategies. p. pages cm.

Lara, A., Solari, M.E., Prieto, M.d.R., Peña, M.P., 2012. Reconstrucción de la cobertura de la vegetación y uso del suelo hacia 1550 y sus cambios a 2007 en la ecorregión de los bosques valdivianos lluviosos de Chile (35° - 43° 30' s). Bosque 33 (1), 13–23. http://dx.doi.org/10.4067/S0717-92002012000100002.

Leblanc, M.J., Tregoning, P., Ramillien, G., Tweed, S.O., Fakes, A., 2009. Basin-scale, integrated observations of the early 21st century multiyear drought in southeast Australia. Water Resour. Res. 45 (4), 1–10. http://dx.doi.org/10.1029/2008WR007333.

Long, D., Scanlon, B.R., Longuevergne, L., Sun, A.Y., Fernando, D.N., Save, H., 2013. GRACE satellite monitoring of large depletion in water storage in response to the 2011 drought in Texas. Geophys. Res. Lett. 40 (13), 3395–3401. http://dx.doi.org/10.1002/grl.50655.

Luebert, F., Pliscoff, P., 2017. Sinopsis bioclimática y vegetacional de Chile. Editor. Univ. 107 (40), 105–107.

Martínez-Vilalta, J., Sala, A., Asensio, D., Galiano, L., Hoch, G., Palacio, S., Piper, F.I., Lloret, F., 2016. Dynamics of non-structural carbohydrates in terrestrial plants: A global synthesis. Ecol. Monograph 86 (4), 495–516. http://dx.doi.org/10.1002/ecm.1231.

Masiokas, M.H., Rabatel, A., Rivera, A., Ruiz, L., Pitte, P., Ceballos, J.L., Barcaza, G., Soruco, A., Bown, F., Berthier, E., Dussaillant, I., MacDonell, S., 2020. A review of the current state and recent changes of the Andean Cryosphere. Front. Earth Sci. 8 (June), 1–27. http://dx.doi.org/10.3389/feart.2020.00099.

Masson-Delmotte, V., Zhai, P., Pirani, A., Connors, S.L., Péan, C., Berger, S., Caud, N., Chen, Y., Goldfarb, L., Gomis, M., et al., 2021. Climate Change 2021: The Physical Science Basis. Cambridge University Press, p. 3949.

Matskovsky, V., Venegas-González, A., Garreaud, R., Roig, F.A., Gutiérrez, A.G., Muñoz, A.A., Le Quesne, C., Klock, K., Canales, C., 2021. Tree growth decline as a response to projected climate change in the 21st century in Mediterranean mountain forests of Chile. Glob. Planet. Change 198 (November 2019), http://dx.doi.org/10.1016/j.gloplacha.2020.103406.

Miranda, A., Lara, A., Altamirano, A., Di Bella, C., González, M.E., Julio Camarero, J., 2020. Forest browning trends in response to drought in a highly threatened mediterranean landscape of South America. Ecol. Indic. 115 (April), 106401. http://dx.doi.org/10.1016/j.ecolind.2020.106401.

Mittermeier, R., Robles, P., Hoffman, M., Pilgrim, J., Brooks, T., Mittermeier, C., Lamoreux, J., Da Fonseca, G., 2004. HOTSPOTS Revisited. In: Comparative Biochemistry and Physiology. Part C, Comparative, no. 1, CEMEX, S.A Toppan Printing Co., Mexico City, Mexico, pp. 1–200. http://dx.doi.org/10.1016/0306-4492(76)90025-3.

Mo, K.C., 2011. Drought onset and recovery over the United States. J. Geophys. Res.: Atmos. 116 (20), 1–14. http://dx.doi.org/10.1029/2011JD016168.

Molina, A., Govers, G., Vanacker, V., Poesen, J., Zeelmaekers, E., Cisneros, F., 2007. Runoff generation in a degraded Andean ecosystem: Interaction of vegetation cover and land use. Catena 71 (2), 357–370. http://dx.doi.org/10.1016/j.catena.2007.04.002.

NASA, 2022. MODIS/Terra-Aqua vegetation indices. URL https://modis.gsfc.nasa.gov/.

Nicolai-Shaw, N., Zscheischler, J., Hirschi, M., Gudmundsson, L., Seneviratne, S.I., 2017. A drought event composite analysis using satellite remote-sensing based soil moisture. Remote Sens. Environ. 203, 216–225. http://dx.doi.org/10.1016/j.rse.2017.06.014.

Nkemdirim, L., Weber, L., 1999. Comparison between the droughts of the 1930s and the 1980s in the southern prairies of Canada. J. Clim. 12 (8 PART 1), 2434–2450. http://dx.doi.org/10.1175/1520-0442(1999)012<2434:cbtdot>2.0.co;2.

Ovenden, T.S., Perks, M.P., Clarke, T.K., Mencuccini, M., Jump, A.S., 2021. Life after recovery: Increased resolution of forest resilience assessment sheds new light on post-drought compensatory growth and recovery dynamics. J. Ecol. 109 (9), 3157–3170. http://dx.doi.org/10.1111/1365-2745.13576.

Parry, S., Prudhomme, C., Wilby, R.L., Wood, P.J., 2016. Drought termination: Concept and characterisation. Prog. Phys. Geogr. 40 (6), 743–767. http://dx.doi.org/10.1177/0309133316652801.

Peters, E., Bier, G., van Lanen, H.A., Torfs, P.J., 2006. Propagation and spatial distribution of drought in a groundwater catchment. J. Hydrol. 321 (1–4), 257–275. http://dx.doi.org/10.1016/j.jhydrol.2005.08.004.

Piao, S., Sitch, S., Ciais, P., Friedlingstein, P., Peylin, P., Wang, X., Ahlström, A., Anav, A., Canadell, J.G., Cong, N., Huntingford, C., Jung, M., Levis, S., Levy, P.E., Li, J., Lin, X., Lomas, M.R., Lu, M., Luo, Y., Ma, Y., Myneni, R.B., Poulter, B., Sun, Z., Wang, T., Viovy, N., Zaehle, S., Zeng, N., 2013. Evaluation of terrestrial carbon cycle models for their response to climate variability and to CO2 trends. Global Change Biol. 19 (7), 2117–2132. http://dx.doi.org/10.1111/gcb.12187.

Potter, N., Saft, M., Western, A., Zhang, L., Peel, M., 2015. Water resources research. J. Am. Water Resour. Assoc. 5 (3), 2. http://dx.doi.org/10.1111/j.1752-1688.1969.tb04897.x.

Preimesberger, W., Scanlon, T., Su, C.H., Gruber, A., Dorigo, W., 2021. Homogenization of structural breaks in the global ESA CCI soil moisture multisatellite climate data record. IEEE Trans. Geosci. Remote Sens. 59 (4), 2845–2862. http://dx.doi.org/10.1109/TGRS.2020.3012896.

Prudhomme, C., Giuntoli, I., Robinson, E.L., Clark, D.B., Arnell, N.W., Dankers, R., Fekete, B.M., Franssen, W., Gerten, D., Gosling, S.N., Hagemann, S., Hannah, D.M., Kim, H., Masaki, Y., Satoh, Y., Stacke, T., Wada, Y., Wisser, D., 2014. Hydrological droughts in the 21st century, hotspots and uncertainties from a global multimodel ensemble experiment. Proc. Natl. Acad. Sci. USA 111 (9), 3262–3267. http://dx.doi.org/10.1073/pnas.1222473110.

Pugnaire, F.I., Morillo, J.A., Peñuelas, J., Reich, P.B., Bardgett, R.D., Gaxiola, A., Wardle, D.A., Van Der Putten, W.H., 2019. Climate change effects on plant-soil feedbacks and consequences for biodiversity and functioning of terrestrial ecosystems. Sci. Adv. 5 (11), 1–12. http://dx.doi.org/10.1126/sciadv.aaz1834.

Qie, L., Lewis, S.L., Sullivan, M.J., Lopez-Gonzalez, G., Pickavance, G.C., Sunderland, T., Ashton, P., Hubau, W., Abu Salim, K., Aiba, S.I., Banin, L.F., Berry, N., Brearley, F.Q., Burslem, D.F., Dančák, M., Davies, S.J., Fredriksson, G., Hamer, K.C., Hédl, R., Kho, L.K., Kitayama, K., Krisnawati, H., Lhota, S., Malhi, Y., Maycock, C., Metali, F., Mirmanto, E., Nagy, L., Nilus, R., Ong, R., Pendry, C.A., Poulsen, A.D., Primack, R.B., Rutishauser, E., Samsoedin, I., Saragih, B., Sist, P., Slik, J.W., Sukri, R.S., Svátek, M., Tan, S., Tjoa, A., Van Nieuwstadt, M., Vernimmen, R.R., Yassir, I., Kidd, P.S., Fitriadi, M., Ideris, N.K.H., Serudin, R.M., Abdullah Lim, L.S., Saparudin, M.S., Phillips, O.L., 2017. Long-term carbon sink in Borneo's forests halted by drought and vulnerable to edge effects. Nature Commun. 8 (1), http://dx.doi.org/10.1038/s41467-017-01997-0.

Salazar, A., Katzfey, J., Thatcher, M., Syktus, J., Wong, K., McAlpine, C., 2016. Deforestation changes land-atmosphere interactions across South American biomes. Glob. Planet. Change 139, 97–108. http://dx.doi.org/10.1016/j.gloplacha.2016.01.004.

Samaniego, L., Thober, S., Kumar, R., Wanders, N., Rakovec, O., Pan, M., Zink, M., Sheffield, J., Wood, E.F., Marx, A., 2018. Anthropogenic warming exacerbates European soil moisture droughts. Nature Clim. Change 8 (5), 421–426. http://dx.doi.org/10.1038/s41558-018-0138-5.

Sawada, Y., 2018. Quantifying drought propagation from soil moisture to vegetation dynamics using a newly developed ecohydrological land reanalysis. Remote Sens. 10 (8), http://dx.doi.org/10.3390/rs10081197.

Schwalm, C.R., Anderegg, W.R., Michalak, A.M., Fisher, J.B., Biondi, F., Koch, G., Litvak, M., Ogle, K., Shaw, J.D., Wolf, A., Huntzinger, D.N., Schaefer, K., Cook, R., Wei, Y., Fang, Y., Hayes, D., Huang, M., Jain, A., Tian, H., 2017. Global patterns of drought recovery. Nature 548 (7666), 202–205. http://dx.doi.org/10.1038/nature23021.

Seguel, O., Luzio, W., Casanova, M., Salazar, O., 2013. The Soils of Chile. p. 185, URL http://www.springer.com/series/8915.

Sepúlveda, M., Bown, H.E., Miranda, M.D., Fernández, B., 2018. Impact of rainfall frequency and intensity on inter- and intra-annual satellite-derived EVI vegetation productivity of an Acacia caven shrubland community in Central Chile. Plant Ecol. 219 (10), 1209–1223. http://dx.doi.org/10.1007/s11258-018-0873-8.

Sheng, Y., Xu, X., 2019. The productivity impact of climate change: Evidence from Australia's Millennium drought. Econ. Model. 76 (July 2018), 182–191. http://dx.doi.org/10.1016/j.econmod.2018.07.031.

Simpson, L., Combettes, P., Müller, C., 2021. c-lasso - A Python package for constrained sparse and robust regression and classification. J. Open Source Softw. 6 (57), 2844. http://dx.doi.org/10.21105/joss.02844.

Tallaksen, L.M.L., Van Lanen, H., Van Lanen, H.A.J., Van Lanen, H., 2004. Hydrological Drought: Processes and Estimation Methods for Streamflow and Groundwater Developments in Water science, Vol. 48, Developmen Elsevier, Amsterdam, theNetherlands: Elsevier Science B.V., p. 579.

Tibshirani, R., 1996. Regression shrinkage and selection via the Lasso. J. R. Stat. Soc. Ser. B Stat. Methodol. 58 (1), 267–288. http://dx.doi.org/10.1111/j.2517-6161.1996.tb02080.x.

Urrutia-Jalabert, R., Barichivich, J., Rozas, V., Lara, A., Rojas, Y., Bahamondez, C., Rojas-Badilla, M., Gipoulou-Zuñiga, T., Cuq, E., 2021. Climate response and drought resilience of Nothofagus obliqua secondary forests across a latitudinal gradient in south-central Chile. Forest Ecol. Manag. 485 (January), http://dx.doi.org/10.1016/j.foreco.2021.118962.

Valdés-Pineda, R., Valdés, J.B., Diaz, H.F., Pizarro-Tapia, R., 2016. Analysis of spatio-temporal changes in annual and seasonal precipitation variability in South America-Chile and related ocean–atmosphere circulation patterns. Int. J. Climatol. 36 (8), 2979–3001. http://dx.doi.org/10.1002/joc.4532.

van Beek, L.P.H., Bierkens, M.F.P., 2009. The Global Hydrological Model PCRGLOBWB: Conceptualization, Parameterization and Verification, Tech.. Techical Report, Utrecht University.

Van Lanen, H.A., 2006. Drought Propagation Through the Hydrological Cycle, no. 308. IAHS-AISH Publication, pp. 122–127.

Van Loon, A.F., 2015. Hydrological drought explained. WIREs Water 2 (4), 359–392. http://dx.doi.org/10.1002/wat2.1085.

Van Loon, A.F., Gleeson, T., Clark, J., Van Dijk, A.I., Stahl, K., Hannaford, J., Di Baldassarre, G., Teuling, A.J., Tallaksen, L.M., Uijlenhoet, R., Hannah, D.M., Sheffield, J., Svoboda, M., Verbeiren, B., Wagener, T., Rangecroft, S., Wanders, N., Van Lanen, H.A., 2016. Drought in the anthropocene. Nat. Geosci. 9 (2), 89–91. http://dx.doi.org/10.1038/ngeo2646.

Venegas-González, A., Juñent, F.R., Gutiérrez, A.G., Filho, M.T., 2018. Recent radial growth decline in response to increased drought conditions in the northernmost Nothofagus populations from South America. Forest Ecol. Manag. 409 (August 2017), 94–104. http://dx.doi.org/10.1016/j.foreco.2017.11.006.

Viale, M., Bianchi, E., Cara, L., Ruiz, L.E., Villalba, R., Pitte, P., Masiokas, M., Rivera, J., Zalazar, L., 2019. Contrasting climates at both sides of the Andes in Argentina and Chile. Front. Environ. Sci. 7 (May), 1–15. http://dx.doi.org/10.3389/fenvs.2019.00069.

Vicente-Serrano, S.M., Cabello, D., Tomás-Burguera, M., Martín-Hernández, N., Beguería, S., Azorin-Molina, C., Kenawy, A.E., 2015. Drought variability and land degradation in semiarid regions: Assessment using remote sensing data and drought indices (1982–2011). Remote Sens. 7 (4), 4391–4423. http://dx.doi.org/10.3390/rs70404391.

Vicente-Serrano, S.M., Gouveia, C., Camarero, J.J., Beguería, S., Trigo, R., López-Moreno, J.I., Azorín-Molina, C., Pasho, E., Lorenzo-Lacruz, J., Revuelto, J., Morán-Tejeda, E., Sanchez-Lorenzo, A., 2013. Response of vegetation to drought time-scales across global land biomes. Proc. Natl. Acad. Sci. USA 110 (1), 52–57. http://dx.doi.org/10.1073/pnas.1207068110.

Vidal, J.P., Martin, E., Franchistéguy, L., Habets, F., Soubeyroux, J.M., Blanchard, M., Baillon, M., 2010. Multilevel and multiscale drought reanalysis over France with the Safran-Isba-Modcou hydrometeorological suite. Hydrol. Earth Syst. Sci. 14 (3), 459–478. http://dx.doi.org/10.5194/hess-14-459-2010.

Wada, Y., Van Beek, L.P., Wanders, N., Bierkens, M.F., 2013. Human water consumption intensifies hydrological drought worldwide. Environ. Res. Lett. 8 (3), http://dx.doi.org/10.1088/1748-9326/8/3/034036.

Wanders, N., Wada, Y., 2015. Human and climate impacts on the 21st century hydrological drought. J. Hydrol. 526, 208–220. http://dx.doi.org/10.1016/j.jhydrol.2014.10.047.

Wilhite, D.A., Glantz, M.H., 2019. Understanding the drought phenomenon: The role of definitions. In: Planning for Drought: Toward a Reduction of Societal Vulnerability. pp. 11–27. http://dx.doi.org/10.4324/9780429301735-2.

Williams, a.P., Seager, R., Abatzoglou, J., Cook, B., Smerdon, J., Cook, E., 2015. Contribution of anthropogenic warming to California drought during 2012 – 2014. Geophys. Res. Lett. 1–10. http://dx.doi.org/10.1002/2015GL064924.Received.

Woolhiser, D.A., Goodrich, D.C., 1988. Effect of storm rainfall intensity patterns on surface runoff. J. Hydrol. 102 (1–4), 335–354. http://dx.doi.org/10.1016/0022-1694(88)90106-0.

Wu, J., Chen, X., Love, C.A., Yao, H., Chen, X., AghaKouchak, A., 2020. Determination of water required to recover from hydrological drought: Perspective from drought propagation and non-standardized indices. J. Hydrol. 590 (June), 125227. http://dx.doi.org/10.1016/j.jhydrol.2020.125227.

Wu, X., Liu, H., Li, X., Ciais, P., Babst, F., Guo, W., Zhang, C., Magliulo, V., Pavelka, M., Liu, S., Huang, Y., Wang, P., Shi, C., Ma, Y., 2018. Differentiating drought legacy effects on vegetation growth over the temperate Northern Hemisphere. Global Change Biol. 24 (1), 504–516. http://dx.doi.org/10.1111/gcb.13920.

Xi, X., Yuan, X., 2022. Significant water stress on gross primary productivity during flash droughts with hot conditions. Agricult. Forest Meteorol. 324 (January), 109100. http://dx.doi.org/10.1016/j.agrformet.2022.109100.

Xie, Z., Duan, A., Tian, Q., 2017. Weighted composite analysis and its application: An example using ENSO and geopotential height. Atmos. Sci. Lett. 18 (11), 435–440. http://dx.doi.org/10.1002/asl.786.

Zhang, S., Yang, Y., Wu, X., Li, X., Shi, F., 2021. Postdrought recovery time across global terrestrial ecosystems. J. Geophys. Res.: Biogeosci. 126 (6), 1–16. http://dx.doi.org/10.1029/2020JG005699.

Zhou, S., Zhang, Y., Williams, A.P., Gentine, P., 2019. Projected increases in intensity, frequency, and terrestrial carbon costs of compound drought and aridity events. Sci. Adv. 5 (1), 1–9. http://dx.doi.org/10.1126/sciadv.aau5740.